Analytica Chimica Acta 881 (2015) 1–23

Contents lists available at ScienceDirect

Analytica Chimica Acta

journal homepage: www.elsevier.com/locate/aca

Review

Electrochemical sensors and biosensors based on redox polymer/carbon nanotube modified electrodes: A review

Madalina M. Barsan, M. Emilia Ghica, Christopher M.A. Brett *

Departamento de Química, Faculdade de Ciências e Tecnologia, Universidade de Coimbra, 3004-535 Coimbra, Portugal

HIGHLIGHTS

- A review of electrochemical (bio) sensors based on redox polymers together with CNT.
- CNT with poly(phenazines) or poly (triphenylmethanes) in different architectures.
- Electrochemical and surface characterization of polymer/CNT modified electrodes.
- Applications based on polymer/CNT modified electrodes as (bio)sensors.

GRAPHICAL ABSTRACT

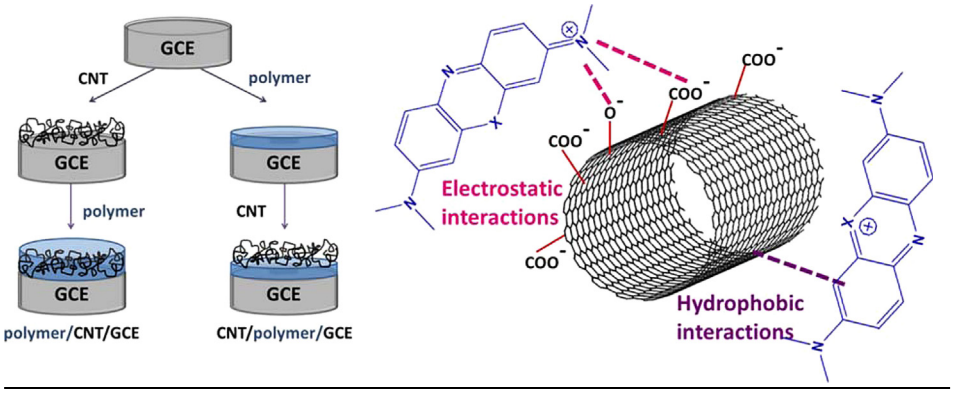

ARTICLE INFO

Article history:
Received 9 December 2014
Received in revised form 20 February 2015
Accepted 22 February 2015
Available online 24 February 2015

Keywords:
Redox polymers
Conducting polymers
Phenazines
Triphenylmethanes
Carbon nanotubes
Electrochemical (bio) sensors

ABSTRACT

The aim of this review is to present the contributions to the development of electrochemical sensors and biosensors based on polyphenazine or polytriphenylmethane redox polymers together with carbon nanotubes (CNT) during recent years. Phenazine polymers have been widely used in analytical applications due to their inherent charge transport properties and electrocatalytic effects. At the same time, since the first report on a CNT-based sensor, their application in the electroanalytical chemistry field has demonstrated that the unique structure and properties of CNT are ideal for the design of electrochemical (bio)sensors. We describe here that the specific combination of phenazine/triphenylmethane polymers with CNT leads to an improved performance of the resulting sensing devices, because of their complementary electrical, electrochemical and mechanical properties, and also due to synergistic effects. The preparation of polymer/CNT modified electrodes will be presented together with their electrochemical and surface characterization, with emphasis on the contribution of each component on the overall properties of the modified electrodes. Their importance in analytical chemistry is demonstrated by the numerous applications based on polymer/CNT-driven electrocatalytic effects, and their analytical performance as (bio) sensors is discussed.

Contents

* Corresponding author. Tel.: +351 239854470; fax: +351 239827703.
E-mail address: cbrett@ci.uc.pt (C.M.A. Brett).

http://dx.doi.org/10.1016/j.aca.2015.02.059
0003-2670/

Madalina Maria Barsan received her Ph.D. degree at University of Coimbra, Portugal, in 2011, where she is currently a Postdoctoral Researcher. Her research interests include the development of new nanostructured electrode materials and methods for biomolecule immobilization for application in biosensors and analytical chemistry.

Mariana Emilia Ghica undertook her Ph.D. at the University of Coimbra, Portugal, in 2007, where she is currently a Postdoctoral Researcher. Her research interests include the development of new nanostructured architectures for electrochemical biosensors for food, clinical and environmental monitoring as well as the HPLC-electrochemical study of the DNA protecting antioxidants in natural extracts.

Christopher Brett is a professor of chemistry at the University of Coimbra, Portugal. His research interests include new nanostructured electrode materials and modified electrode surfaces, electrochemical sensors and biosensors, electroactive polymers, corrosion and its inhibition, and applications of electrochemistry in the environmental, food and pharmaceutical areas.

Nomenclature

Symbol glossary

AA	Ascorbic acid
ACNT	Aligned carbon nanotubes
AFM	Atomic force microscopy
AlcDH	Alcohol dehydrogenase
AuNP	Gold nanoparticles
BEP	Buckeye paper
C8-LPEI	Octylmodified-linear poly(ethylenimine)
CCE	Carbon composite electrode
Ccl	Carbon cloth
CFE	Carbon film electrode
chit	Chitosan
CILE	Carbon ionic liquid electrode
CNT	Carbon nanotubes
CPE	Constant phase element
CV	Cyclic voltammetry
DA	Dopamine
DH	Dehydrogenase
DHP	Dihexadecyl hydrogen phosphate
DMF	Dimethylformamide
DNA	Deoxyribonucleic acid
DPV	Differential pulse voltammetry
DSDH	D-sorbitol dehydrogenase
EDC	1-Ethyl-3-(3-dimethylaminopropyl)carbodiimide
EIS	Electrochemical impedance spectroscopy
$E^{\Theta'}$	Formal potential
E_m	Midpoint potential
EP	Epinephrine
E_p	Peak potential
EPPG	Edge-plane pyrolytic graphite
eV	Electron volt
FAD	Flavin adenine dinucleotide
GCE	Glassy carbon electrode
GlcDH	Glucose dehydrogenase
GOx	Glucose oxidase
HRP	Horsereadish peroxidase
I_{max}	Maximum current
ITO	Indium tin oxide
KHP	Potassium hydrogen phthalate
K_M	Michaelis–Menten constant
LDH	Lactate dehydrogenase
MWCNT	Multiwalled CNT
NAD^+	Nicotinamide adenine dinucleotide
NHS	*N*-Hydroxysuccinimide
PAA	Poly(azure A)
PAB	Poly(azure B)
PAMAM	Poly(amido amine)dendrimer
PBCB	Poly(brilliant cresyl blue)
PBG	Poly(brilliant green),
PBS	Phosphate buffer saline
PDDA	Poly(diallyldimethylammonium chloride)
PEI	Poly(ethylenimine)
PMalG	Poly(malachite green)
PMB	Poly(methylene blue)
PMG	Poly(methylene green)
PNB	Poly(Nile blue)
PNR	Poly(neutral red)
PPhS	Poly(pheno-safranin)
PPyr	Poly pyrrole
PTBO	Poly(toluidine blue O)
PTH	Poly(thionine)
R_{ct}	Charge transfer resistance
RNA	Ribonucleic acid
SCE	Saturated calomel electrode
SEM	Scanning electron microscopy
SPCE	Screen printed carbon electrode
SWCNT	Single-walled carbon nanotubes
SWNH	Single walled nanohorns
TEOS	Tetraethyl orthosilicate
UA	Uric acid
ν	Scan rate
v/v	Volume per volume
w/v	Weight per volume
Γ	Surface coverage

1. Introduction

Conducting/electroactive polymers and carbon nanotube (CNT) matrices have received considerable attention in recent years in the bioanalytical sciences due to their important role in enhancing the sensitivity and electrocatalytic activity of the corresponding sensor devices.

Conducting polymers, in particular, have been widely used in bioanalytical applications due to their inherent charge transport properties and biocompatibility, in biosensor applications showing advantages owing to their specific sensitivity to very minor perturbations. The controlled synthesis of polymers is made possible by electropolymerization, by adjusting the electropolymerization parameters, e.g., cyclic voltammetric scans, scan rate, applied potential, being a simple but prevailing method for the selective modification of electrodes with desired polymer designs for application in sensing [1,2].

Besides conducting polymers, CNT, among other carbon based nanomaterials (carbon nanohorns, fullerenes, graphene) are also being extensively used in (bio) sensor construction due to their dimensional and chemical compatibility with (bio) molecules, which enables them to catalyze reactions [3] and to promote electron-transfer reactions between biomolecules and electrode substrates [4–8]. Functionalization of CNT, which occurs on the side wall defects, tips, and other non-hexagonal regions, is required for their dispersion and solubilisation, and for further processing and applications [9]. Traditional chemical methods include non-covalent functionalization with surfactants or polymers, covalent functionalization by oxidation and direct chemical functionalization of the side walls using addition [10]. Other chemical methods, also being investigated, include the grafting of multi walled CNT (MWCNT) by monomers or polymers [9,11]. CNT functionalization by polymers occurs by covalent reactions between the long polymer chains and CNT, known as polymer grafting. Polymers can be either “grafted to” or “grafted from” CNT, in the first case monomers being initially immobilized onto the CNT, followed by in-situ polymerization and in the second case attaching functionalized polymer molecules to the functionalized CNT via chemical reactions [9].

The combination of CNT with polymers is beneficial, since CNT can improve the electrical conductivity and mechanical strength of the resulting polymer-CNT hybrids, because of their unique properties and their geometry, which provides a three-dimensional nanostructure with a large electroactive area [12]. Polymers can be formed by electropolymerization on electrodes previously modified with CNT, they can be co-immobilized on the electrode together with CNT during electropolymerization, from a dispersion of CNT and soluble monomer in water, or electropolymerization of a previously synthesized CNT functionalized with monomers can be carried out [13].

Interaction between CNT and monomers/polymers is an important factor in the construction of robust CNT/polymer based nanocomposite modified electrodes. CNT exhibit a special sidewall curvature and a π-conjugative structure with a highly hydrophobic surface, which allow them to interact with aromatic compounds, through π–π electronic and hydrophobic interactions [14–17]. The interactions can also be electrostatic, following CNT functionalization, which can be done in such a way as to produce a surface that is either negative, as is the case of the frequently used acidic functionalization which provides $-COO^-$ groups [18], or positive, as is the case of amino-functionalized CNT [19–21].

Conducting polymer/CNT composites have been very much used in (bio) sensor construction [1,13]. This specific combination leads to an improved performance of the resulting sensing devices, because of their complementary electrical, electrochemical and mechanical properties, and also due to synergistic effects [6,7]. The use of a redox mediator in combination with CNT can lead to a sensor with significant catalytic properties [22,23]. Among the redox mediators, the group of azines, which can form electroactive polymers, such as phenazines, phenothiazines, phenoxazines, etc., have wide application in (bio) electrochemistry in the construction of new (bio) sensors [24–26], and have been used together with CNT in a variety of sensor and biosensor platforms, which will be reviewed.

The order of deposition of the carbon nanotubes or electroactive polymer, as well as their relative amounts, can influence the performance as sensors, as is visible in the diagram in Fig. 1. Which order of deposition will give the best sensor performance and the best synergistic effects can vary. If CNT are deposited first, then the speed of movement of the monomer within the CNT network during electropolymerization will influence polymer growth, and will depend on its size and geometry and ease of nucleation on the electrode substrate or surface of the CNT. If the polymer is deposited first, the degree of porosity will influence the physical entry of CNT to within the upper part of the polymer structure.

Polyphenazines and poly(triphenylmethanes) used in combination with CNT, for (bio) sensing and fuel cell applications are: poly(azure A), poly(azure B), poly(brilliant cresyl blue), poly (methylene blue), poly(methylene green), poly(Nile blue), poly (neutral red), poly(phenosafranin), poly(thionine) and poly(toluidine blue O); poly(triphenylmethanes) are poly(brilliant green) and poly(malachite green). The chemical structures of these monomers are shown in Fig. 2. The preparation of the corresponding modified electrodes, including CNT pre-treatment/immobilization and polymer deposition on bare and CNT-modified electrodes will be discussed, stressing the influence of CNT on the polymerization process. The electrochemical and surface characterization of polymer/CNT modified electrodes is presented in detail, with emphasis on the contribution of each component to the overall electrochemical properties of the modified electrodes. Finally, applications based on polymer/CNT modified electrodes for the detection of common analytes, with a description of analytical parameters and the analytical method utilized, will be presented in tables and discussed.

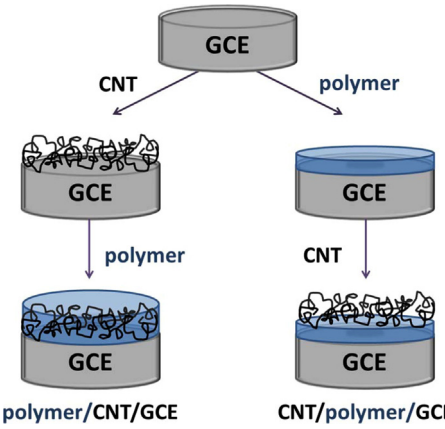

Fig. 1. Schematic preparation of CNT/polymer modified electrodes.

2. Preparation of CNT/polymer or polymer/CNT electrodes

This section provides detailed information about the functionalization of CNT [27–29], their dispersion in different media and immobilization on bare or polymer modified electrodes. The polymerization procedures of monomers will also be described, namely of BCB [30–37], BG [38–40], MalG [41–44], MB [45–52], MG [53–60], NB [61–66], NR [31,67–73], TH [40,74–82], TBO [83–91], azure A [92], AB [93,94] and PhS [95], indicating the monomer solution content and experimental parameters used. Lastly, the polymerization profile of monomers on bare and on CNT-modified electrodes will be discussed and compared, with emphasis on the influence of CNT on the polymerization process.

2.1. Functionalization and dispersion of CNT

Due to their hydrophobic nature, the functionalization of CNT is often required prior to their use, in order to ensure a homogeneous dispersion [27]. Moreover, as-synthesized CNT are generally impure [28] and the treatment used for their functionalization also removes the impurities [29]. Usually, the functionalization consists in acidic treatment with either a mixture of concentrated acids (H_2SO_4:HNO_3) [32,44,45,48,68,75–77,80,93], or with concentrated HNO_3 [31,38–40,50,63–65,71,72,83,84,86,92]. MWCNT were hydrophilized by grinding MWCNT together with solid KOH [7,69] or were doped with K by using a dimethoxyethane solution containing phenanthrene [49]. CNT can be purchased in the carboxylated form [81,85], or as amino functionalized CNT [70].

CNT have been usually dispersed with the aid of ultrasonication in water (or buffer solutions), [7,31,32,36,37,45,69,70,75,79,80,83,84,86,89,92,93], DMF [47,48,50,53,60–65,72,78,79,81,85,95], chitosan solution [31,38–40,57–59] or ethanol [44,49,68]. Nafion® has been used as an alternative to overcome the drawbacks of chemical functionalization and physical (milling) dispersion of CNT, the dispersion occurring due to hydrophobic interaction between Nafion® and CNT, as illustrated in Fig. 3 [41,42,56,77]. Other methods include the use of surfactants, such as dihexadecyl hydrogen phosphate (DHP) [37], a DMF/ethanol mixture [71] or a gelatin aqueous solution [87,88].

2.2. Polymerization parameters

2.2.1. Poly(brilliant cresyl blue) – PBCB

Brilliant cresyl blue (BCB) was electropolymerised on top of CNT-modified electrodes mostly by potential cycling in the range −0.7 to +1.2 V vs. SCE, for 15–30 cycles, at a scan rate of 50 or 100 mV s^{-1} [30,31,34–36]. The polymerization solution used as supporting electrolyte was usually 0.1 M PBS, pH ~7.0, with the addition of 0.1 M KCl in [30], or 0.1 M KNO_3 [31,33], the monomer concentration ranging from 0.1 to 2.5 mM. A typical polymerization profile is presented in Fig. 4.

In [37] the authors report the co-deposition of MWCNT with PBCB. In this case, equal amounts of monomer solution and CNT suspension in DHP were mixed and the electrode was drop cast with the BCB + MWCNT + DHP mixture, followed by polymerization by CV in 0.1 M NaPBS + 0.1 M $NaNO_3$ between −0.8 and 1.0 or 1.8 V vs. SCE, for 5–20 cycles at 50 mV s^{-1}.

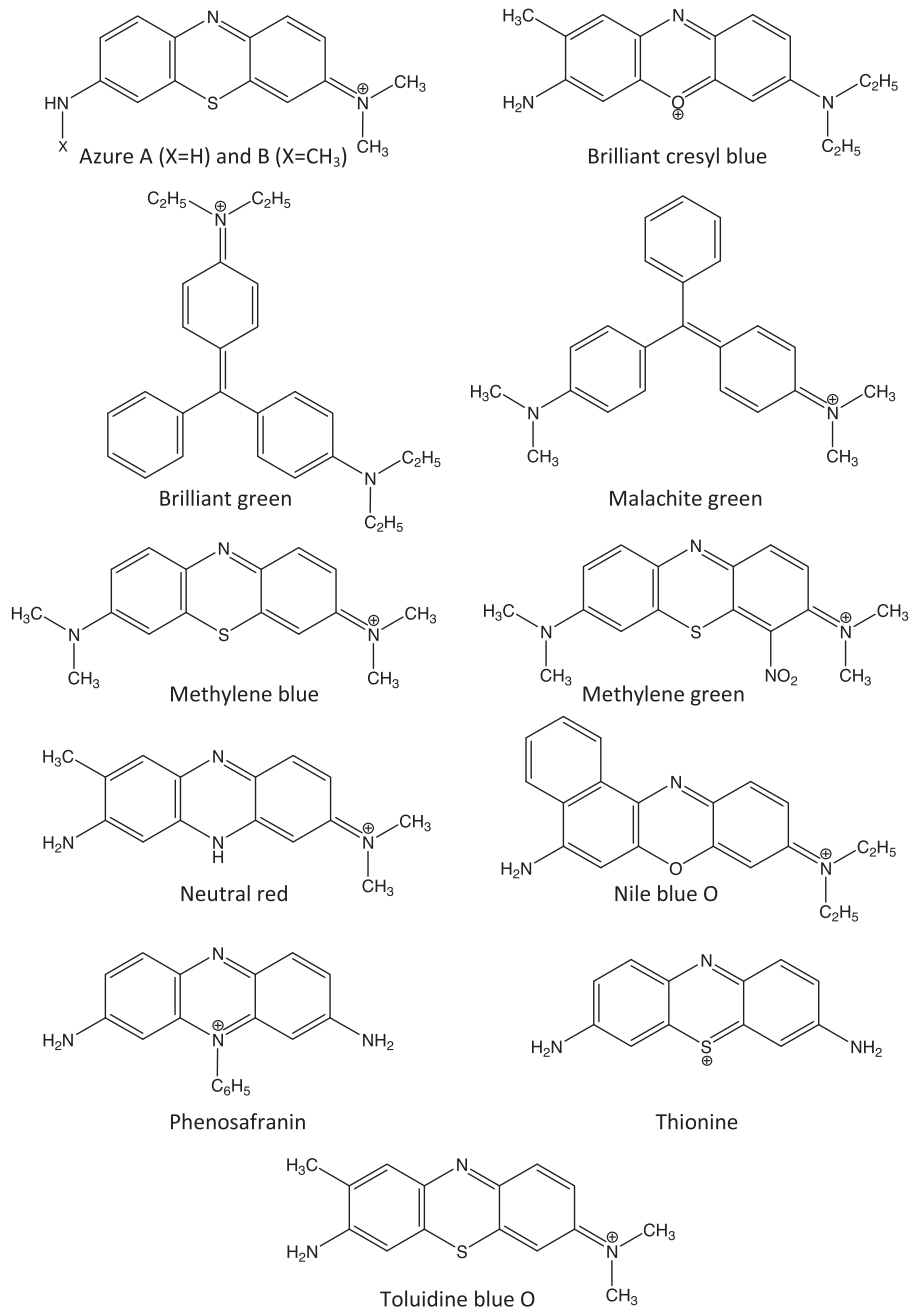

Fig. 2. Chemical structures of phenazine and triphenylmethane monomers.

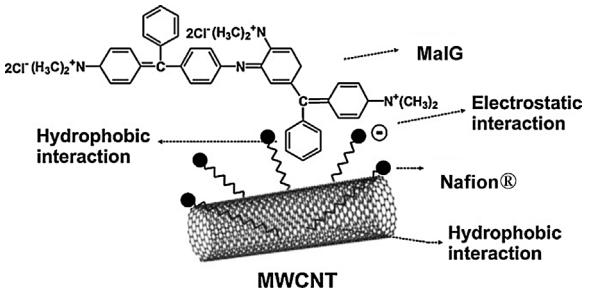

Fig. 3. Possible interaction between CNT, Nafion (NF) and MalG. From [41], reproduced by permission of Elsevier.

Potentiostatic deposition of PBCB was reported in [32,33] by applying a fixed potential of +0.9 V vs. SCE to SWCNT/GCE for 75 s [33] or 90 s [32] in 0.5 mM BCB + 0.1 M KNO_3 + 0.1 M PBS pH 8.0.

2.2.2. Poly(brilliant green) – PBG

The polymerization conditions of BG were optimized on bare CFE. The polymerization solution contained 0.1, 0.5 or 1.0 mM BG in either 0.1 M H_2SO_4 or McIlvaine's buffer with different pH values, the last leading to thicker films. Polymerization was done by potential cycling between −1.0 and +1.2 V vs. SCE at 100 mV s^{-1} during 5 or 10 cycles [38–40]. Polymerization on top of CNT was performed using the optimized procedure, in 1 mM BG + McIlvaine's buffer pH 4.0, for 20 cycles [38,40].

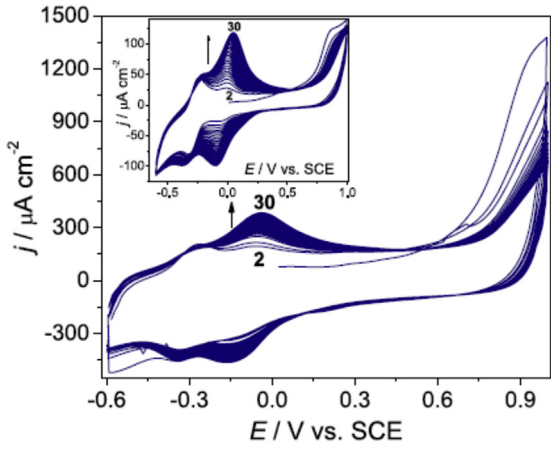

Fig. 4. Polymerization of BCB at MWCNT/GCE and GCE in inset from 0.1 mM BCB in 0.1 M PBS pH 7.0 + 0.1 M KNO_3. From [31], reproduced by permission of Springer.

2.2.3. Poly(malachite green) – PMalG

The polymerization of MalG was performed using different experimental conditions. The first used 0.5 mM MalG in 10 mM potassium hydrogen phthalate (KHP) pH 4.0 + 0.1 M Na_2SO_4, by potential cycling between −0.3 and 1.4 V for 25 cycles [41], the second used 5 mM MalG in H_2SO_4 pH 1.5 between 0 and 1.2 V for 25 cycles [42], and the third, 10 mM MalG in 0.025 M NaPBS pH 6.0 + 0.5 M $NaNO_3$, between −1.4 and 1.8 V for 25 or 12 cycles [44]. In [43], MWCNT were dispersed in a MalG solution and dropped onto a GCE surface, followed by polymerization.

2.2.4. Poly(methylene blue) – PMB

The polymerization of MB was done by using potential cycling [45–50] and by applying a fixed potential of +0.9 V [51]. Different polymerization solutions were used: 1.0 mM MB [45], 0.1 mM MB + 0.1 M PBS pH 7.0, [47,51], 2 mM MB + TRIS buffer pH 7.6 [48], 1 mM + PBS [49] and 1 mM MB + 0.025 M $Na_2B_4O_7$ + 0.1 M Na_2SO_4 pH 9.2 [50]. The potential was cycled between negative and positive potential limits in the range −0.7 to 1.2 V, the optimum being from −0.7 to 1.0 V, for 30 scans. In [46], PMB was formed on CNT-ionic liquid paste electrodes. In [45,47–49] the authors used neutral solutions for polymerization, the CVs recorded during polymerization [47,49] clearly showing less effective polymerization compared with that reported in [50], in which alkaline medium was used in the presence of sulphate ions (see Fig. 5), the same as in [52]. It has been reported that for phenothiazine dyes, such as MB and MG, polymerization occurs better in alkaline media, than in neutral or acidic media [52].

2.2.5. Poly(methylene green) – PMG

The polymerization solutions contained the monomer at a concentration of either 0.4 or 0.5 mM in 10 mM $Na_2B_4O_7$ + 0.1 M $NaNO_3$ [53,54,56,60] or in PBS with added nitrate ions [55,57] or chloride ions [58,59], in some cases the solution being deoxygenated before polymerization [54,55,57]. The potential ranges used were −0.5 up to 1.2, 1.3 or 1.5 V [53,55,57–60], or −0.3 to 1.3 V [54,56] at 50 mV s^{-1}, usually for 10 cycles. Film growth is faster in alkaline media, rather than in slightly acidic or neutral media.

2.2.6. Poly(Nile blue) – PNB

Electropolymerization on GCE and SWCNT/GCE was done using 0.5 mM NB solution in PBS, pH 8.3 by cycling between −0.8 and +1.2 V for 10 cycles at 100 mV s^{-1} [61,62]. It was found that by dipping the SWCNT/GCE into the NB monomer solution for 30 min, the monomer adsorbs into the structure, due to the π–π electronic and/or hydrophobic interactions [66].

PNB was polymerized either before or after coating with MWCNT, from 0.5 mM NB in PBS pH 6.0 between −0.6 and 1.2 V vs. SCE at 50 mV s^{-1}. Five polymerization cycles were used on GCE and 17 on MWCNT/GCE [63–65], as shown in Fig. 6. In [65], five cycles were used for the polymerization of NB, since thicker PNB films, obtained with more than 5 cycles, on top of MWCNT coatings, led to unstable surface modifier films [63].

2.2.7. Poly(neutral red) – PNR

Polymerization of NR has been carried out in a number of different media, usually slightly acidic. It was performed in 1 mM NR + 0.025 M KPB + 0.1 M KNO_3 pH 5.5 from −1.0 to +1.0 V vs. SCE at 50 mV s^{-1} for 15 or 20 cycles [31,72], using a procedure previously optimized in [73]. A typical CV recorded during polymerization using this procedure is shown in Fig. 7. A similar polymerization solution was used in [68], with less monomer, 0.1 mM. The scan rate was rather low, limiting the number of cycles to 6, chosen with the aim of obtaining a smooth and compact film. Five bilayers of MWCNT/PNR were formed by alternately dropping an MWCNT dispersion on GCE and electrodepositing PNR, constructing {MWCNT/PNR}$_5$/GCE [68].

In other work, polymerization of NR was performed on MWCNT/GCE in 0.05 mM NR + 0.1 M potassium hydrogen phthalate (KHP) pH 4.0, 0.05 mM NR + H_2SO_4 pH 1.0, [7,69] or 0.05 mM NR + 0.1 M PBS pH 6.0 [69]. The potential was cycled between −0.7 and 1.0 V, for 20 scans at 100 mV s^{-1} [7,69].

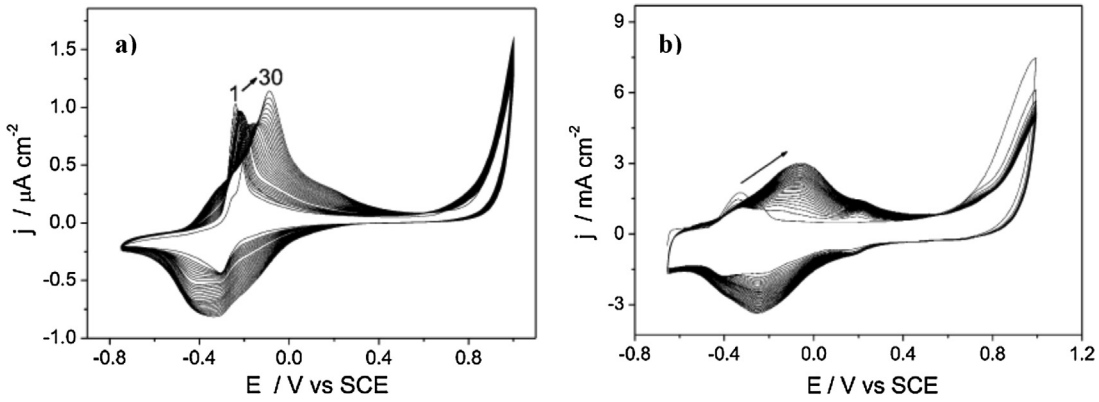

Fig. 5. Cyclic voltammograms recorded during the polymerization of MB at (a) CCE and (b) MWCNT/CCE electrodes from 1 mM MB in 0.025 $Na_2B_4O_7$ + 0.1 M Na_2SO_4 pH 9.2; υ = 50 mV s^{-1}. From [50], reproduced by permission of Wiley.

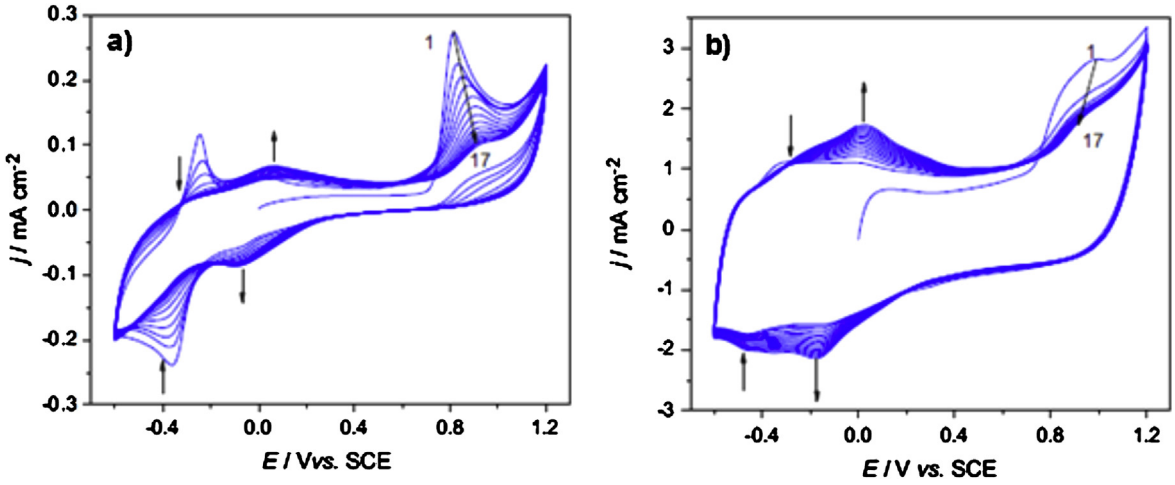

Fig. 6. Polymerization of NB from 0.5 mM NB in 0.1 M PBS pH 6.0; $\nu = 50\,mV\,s^{-1}$ (A) on GCE for 5 scans and (B) on MWCNT/GCE for 17 scans. From [63], reproduced by permission of Elsevier.

LbL deposition of PNR was reported in [67], the first negative layer being of PNR/Nafion®, followed by positively charged chitosan and negatively charged acid-functionalized MWCNT. Amino-functionalized MWCNT, previously adsorbed on GCE, were used as substrate for NR polymerization in 0.1 mM NR + 10 μM FAD in PBS pH 7.0 at 100 mV s^{-1} for 30 cycles, during which negatively charged FAD is adsorbed on the positively charged PNR, forming a hybrid material [70].

A nano-Pt-PNR/MWCNT modified electrode was obtained by polymerizing NR on MWCNT/GCE in 5.0 mM NR + 0.5 M H_2SO_4 + 0.1% (v/v) H_2PtCl_6, by cycling between −0.2 and 1.4 V for 25 cycles at 50 mV s^{-1} [71].

2.2.8. Poly(thionine) – PTH

TH was polymerized under different polymerization conditions by potential cycling. It was polymerized on a MWCNT-modified carbon containing ionic liquid electrode (CILE) in 0.5 mM TH + 0.1 M PBS pH 6.5, by cycling between −0.5 and +0.1 V at 100 mV s^{-1} for 40 cycles [75], a procedure perfected in [82]. Similarly, PTH was deposited on MWCNT/GCE or MWCNT/AuNP/GCE in 5 mM TH + 0.1 M PBS pH 6.0–7.0, by cycling 40 times between –0.4 and 0.4 V at 50 mV s^{-1} [78,79]. Low pH solutions were used in [76] and [80], when TH was polymerized at MWCNT/GCE in 0.4 mM TH +0.5 M H_2SO_4 solution, by cycling between −0.4 and 1.1 V vs. SCE [76]. AuNP were adsorbed into a PTH film by soaking the PTH/MWCNT/GCE in colloidal AuNP suspension, following PTH formation in 4 mM TH + 4.4 M acetic acid solution pH 1.9, between −0.2 and 1.4 V for 30 cycles [80].

The best polymerization procedure was found to be in alkaline solutions, as for other phenothiazines, in 1 mM TH + 0.025 M $Na_2B_4O_7$ + 0.1 M KNO_3, pH 9.0 between −1.0 and 1.0 V vs. SCE, at 50 mV s^{-1} for 30 scans [40]. PTH was also formed in organic media in 1.0 mM TH in ACN solution (deoxygenated), by cycling from 0.0 to 1.4 V vs. SCE at 40 mV s^{-1} for 40 cycles [74] or together with glutaraldehyde (GA) in 0.1 mM thionine +2.5% GA CV between −0.4 and +0.4 V at 50 mV s^{-1} [77].

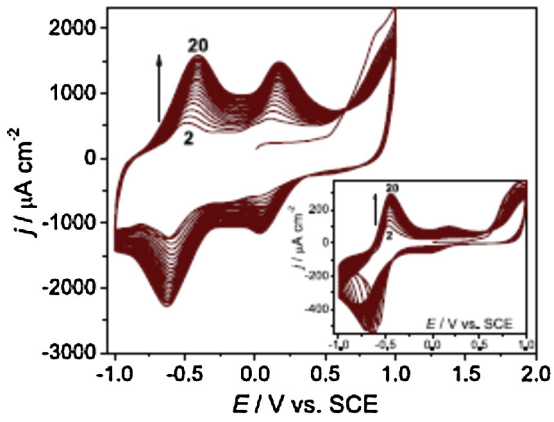

Fig. 7. CVs recorded during polymerization of NR at MWCNT/GCE in 1 mM NR + 0.025 M KPB + 0.1 M KNO3 (pH 5.5) from −1.0 to + 1.0 V vs. SCE at 50 mV s^{-1}; in inset polymerization at bare GCE. From [31], reproduced by permission of Springer.

2.2.9. Poly(toluidine blue O) – PTBO

TBO was polymerized on MWCNT/GCE in 5 mM TBO in PBS pH 7.4, by cycling between −0.76 and 1.0 V at 50 mV s^{-1} for 20 cycles [83], a procedure previously developed in [90,91], as seen in Fig. 8, or between −0.3 and 1.0 V [84]. The same electrolyte, but with only 0.3 mM TBO, was used in [87], when polymer was deposited with zirconia nanoparticles on a gelatin-MWCNT film, a film similar to that reported in [88], the potential being cycled at 100 mV s^{-1}, between −0.6 and 1.0 V vs. Ag/AgCl for 20 cycles. Another procedure was to use a solution of 0.4 or 0.5 mM TBO + 0.01 M $Na_2B_4O_7$ + 0.1 M $NaNO_3$, between −0.6 and 1.1 or 1.5 V, at 50 mV s^{-1} [85,89], first reported in [26].

In [86], the TBO/MWCNT adduct modified electrode was transferred to McIlvaine buffer solution pH 4.0 and PTBO was obtained directly on MWCNT, by potential cycling between −0.6 V and +1.0 V at 50 mV s^{-1} for 30 cycles.

2.2.10. Poly(azure A) and poly(azure B) – PAA and PAB

PAA has been deposited on SWCNT/GCE or on bare GCE on which azure A was adsorbed by immersing the electrodes in 5.0 mM azure A solution for 2 h, azure A then being polymerized by cycling between −0.5 V and +0.9 V at 50 mV s^{-1} in PBS pH 6.5 for 40 cycles [92].

In a multilayer LbL procedure, a thin layer of PAB was formed on the electrode substrate to ensure a positively charged surface [93]. Multilayers of MWCNT and poly(diallyldimethylammonium chloride) (PDDA) were then deposited by alternately dipping the electrode (for 30 min) into a 0.1% w/v MWCNT negatively charged dispersion and in a 1.0% w/v aqueous solution of positively charged PDDA containing 0.5 M NaCl. Finally, AB was polymerized on top of

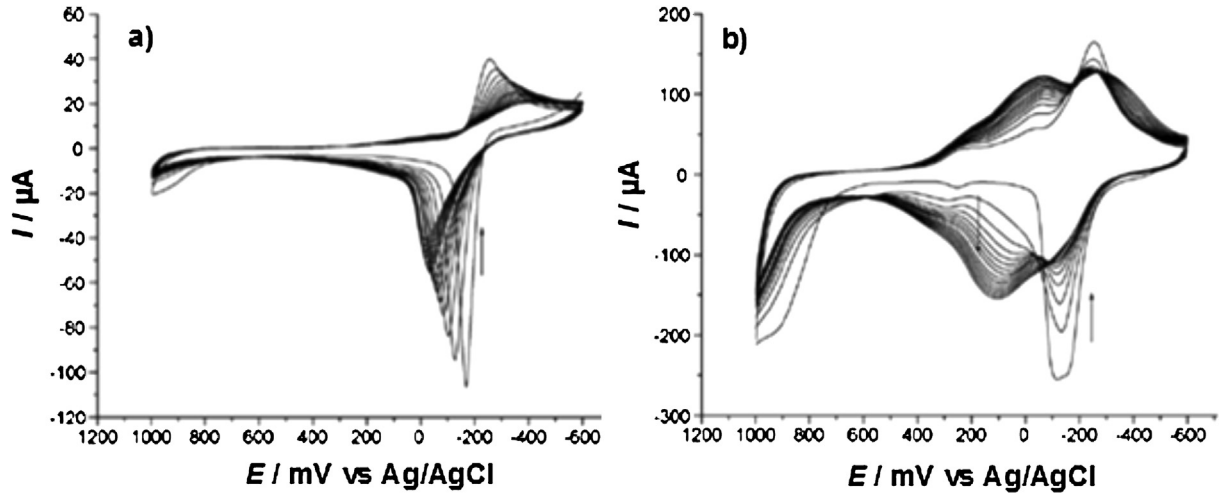

Fig. 8. CVs recorded during polymerization of TBO at (a) MWCNT/GCE and (b) GCE in a solution containing 5 mM TBO in PBS pH 7.4; $\nu = 50\ mV\ s^{-1}$. From [83], reproduced by permission of Elsevier.

$\{MWCNT/PDDA\}_n$/GCE, to form $\{PAB/MWCNT/PDDA\}_n$/GCE, by cycling in deoxygenated 0.1 mM AB + PBS, between −0.5 and 1.1 V at 50 mV s^{-1}, for 10 cycles, a polymerization procedure similar to that reported earlier in [94].

2.2.11. Poly(phenosafranin) – PPhS

Phenosafranin has been polymerized on top of a SWCNT/EPPG electrode in a solution containing 0.5 mM monomer +0.2 M H_2SO_4 by potential cycling between −0.5 and 1.3 V for 3 cycles at 50 mV s^{-1} [95].

2.3. Electropolymerization profiles

The crucial step of the electropolymerization process is the formation of radical cations generated in an irreversible oxidation, which initiates the polymerization [37,65,80,91,95–99], the formation of radicals becoming less evident after several cycles, as manifested by a decrease in the corresponding peak currents [38,39,41]. The reversible signal ascribed to the monomer redox activity usually is located at negative potentials, decreases and reaches a steady value [30–35,48,50–52,61,65,83,84,86,92,93]. A new redox couple appears at potentials that are more positive than that of the monomer and increases on cycling, being attributed to polymer deposition (Figs. 4–6) [30–35,48,50–52,65,83,84,86,92, 93,96]. However, in some cases monomer and polymer redox couples occur at the same potential, as in the case of PBG, PMalG, PNR, PTH, and PPhs exemplified in Fig. 7.

As expected, the presence of CNT leads to a greater coverage by the polymer, since CNT provide more surface area than bare electrodes, and also due to possible interactions between monomer and CNT [32,62,100] as shown in Fig. 3, expressed by higher electropolymerization currents at CNT-modified electrodes [7,30,31,38,41,42,60,61,65,69,92,93]. For this reason, the active surface coverage concentration calculated for the polymer, Γ, is higher on CNT modified electrodes [41,42]. In some cases, polymer formation was recorded as continuing for a larger number of cycles on CNT-modified electrodes, compared to the bare ones [31,38,61,65]. BCB and BG polymerization on CNT-modified electrodes occurs at a potential 50–100 mV less positive than on bare electrodes [31,38]. Regarding NR polymerization on CNT/GCE, the second pair of peaks, at ~0.1 V, is much more evident than on bare electrodes [7,7,31,69,72]; a similar polymerization profile of NR was observed on porous graphite composite electrodes [97], which was attributed to the porous nanostructured substrate. The formal potentials of monomers and the corresponding polymers are listed in Table 1.

There is only a small or no influence from other components present in the electrode architecture on the electropolymerization profiles to form the films. However, and as an example, NR polymerization in the presence of H_2PtCl_6 at MWCNT/GCE, showed redox couples shifted slightly toward more negative potentials compared to those recorded in the absence of H_2PtCl_6, due to the high conductivity of the resulting nano-Pt-PNR copolymer film [71]. Nevertheless, when NR was copolymerized with FAD, exactly the same redox couples were recorded with an extra one corresponding to FAD at −0.42 V [70]. PTH deposition was similar in the presence of AuNP, with slightly higher currents [78]. Similarly, nanoparticles of ZrO_2 together with MWCNT did not influence the polymerization of TBO [87].

3. Characterisation of polymer/CNT modified electrodes

Poly(phenazine)/CNT and poly(triphenylmethane)/CNT films formed on different electrode substrates have been characterized using various techniques, namely electrochemical: cyclic voltammetry, and impedance spectroscopy, and microscopic: scanning electron, scanning tunneling, transmission electron and atomic force microscopy. The characteristics of polymer/CNT architectures will also be compared with those of only polymer.

Table 1
Approximate formal potential values, to the closest 100 mV, of phenazine and triphenylmethane monomers $E^{\Theta'}_{monomer}$, and polymers, $E^{\Theta'}_{polymer}$, expressed in *V* vs. SCE.

Polymer	$E^{\Theta'}_{monomer}$/V vs. SCE	$E^{\Theta'}_{polymer}$/ V vs. SCE	Reference
PBCB	−0.3	0.0	[30–35]
PBG	0.5	0.5	[38,39]
PMalG	0.5	0.5	[42]
PMB	−0.3	0.0	[48,50–52]
PMG	0.0	0.2	[52]
PNB	−0.4	0.0	[61,65]
PNR	−0.5	−0.5	[69,72]
PTH	−0.3	−0.3	[75,76,78,79]
PTBO	−0.2	0.1	[83,84,86]
PAA	−0.3	−0.1	[92]
PAB	−0.2	0.0	[93,94]
PPhS	0.0	0.0	[95]

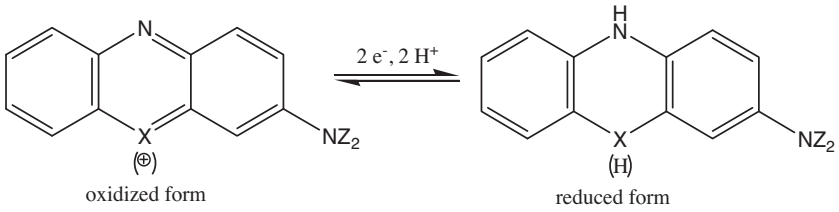

Scheme 1. Oxidation–reduction of phenazines; X=N, S, O; Z=H, $-CH_3$,$-C_2H_5$.

3.1. Cyclic voltammetry (CV)

As seen previously, potential cycling is the principal method for preparation of the polymer/CNT modified electrodes, and cyclic voltammetry is the predominant technique used for characterisation of the films formed. Different aspects have been investigated, such as electrochemical profile, kinetics, scan rate dependence, influence of pH and film stability.

3.1.1. Electrochemical profile and kinetics

Cyclic voltammograms for poly(phenazine)/CNT and poly (triphenylmethane)/CNT modified electrodes have been recorded in different media, at different pH values between 5.3 and 8.3 [32,39,62,63,72,76,86,89,92,93]. Independent of pH and scan rate, CVs exhibit two redox couples at electrodes covered with polymers both in the absence or presence of nanotubes, the couple with more negative formal potential corresponding to the reaction of monomer units contained in the redox polymer structure, while the more positive couple represents the redox reaction of the nitrogen bridges present [101,102]. For NR and PS, the monomer and polymer redox reaction occur at similar potentials [31,95]. The oxidation–reduction mechanism of phenazines involves 2 protons and 2 electrons as briefly described in Scheme 1.

The peak-to-peak separation for both couples is normally small, less than 90 mV for PBCB/GCE and PBCB-MWCNT/GCE [35], showing fast electron transfer. An increase in peak currents obtained at polymer/CNT modified electrodes by a factor of 2 [86] or 5 [92], compared with the polymer modified electrode, indicates the first as a better electroactive platform [35]. This phenomenon may be ascribed to the fact that CNT possess higher electrical conductivity than GCE, which benefits the polymerization, as well as a π-conjugative structure with a highly hydrophobic surface, which allows good interaction between CNT and aromatic compounds, through π–π electronic and/or hydrophobic interactions to form nanocomposites [62]. The values of the peak potentials are slightly more negative at polymer/CNT/electrode than those at polymer/electrode [62], which has been ascribed to the fact that CNT can act as promoters to enhance the electrochemical reaction, increasing the rate of the heterogeneous electron transfer and decreasing the overpotential [103].

The effect of the position of the CNT, on top of the polymer or beneath it has been studied and it was observed that redox peaks were higher when polymer was formed on top of the nanotubes [50,63], e.g., Fig. 9 for PNB. This is probably due to the fact that the counterion access to the polymer is hindered when covered by nanotubes, see Fig. 1. An exception is the case of PBG, for which very similar current values were found at PBG/MWCNT/CFE and MWCNT/PBG/CFE [39], but this can be explained by the weak polymerization of BG on top of the nanotubes.

Cyclic voltammetry was used to investigate GCE modified with PTH deposited on different CNT, namely MWCNT, MWCNT–COOH, SWCNT–COOH and aligned carbon nanotubes (ACNT) [81]. All PTH/CNT modified electrodes gave a significantly enhanced double-layer capacitance current in the sequence: MWCNT–COOH > ACNT > SWCNT–COOH > MWCNT. The lowest current at non-functionalized MWCNT is due to the fact that the ends of the nanotubes are closed, which does not allow the monomer to enter inside for better polymerization. On the other hand, MWCNT–COOH have open tips and a more disordered conformation, which permit more polymer to be formed on top, hence the highest current is exhibited at these nanotubes. The roles of the individual components and the possible synergistic effects in promoting electron transfer were investigated by comparing the electrochemical behavior of $K_3Fe(CN)_6$ at different platforms with poly (phenazines) with or without CNT. For PTH, both on top and beneath the CNT, an increase of the peak heights as well as of the reversibility of the redox probe was observed [74,75,77].

The kinetic characteristics of the modified electrodes were also investigated by cyclic voltammetry and the standard rate constant of the surface reaction, k_s, was obtained from Laviron's equation [104]. Faster electron transfer was observed when CNT were present in the electrode architecture [41,49,75], three times higher at the PTH/MWCNT/CILE and PMalG/MWCNT/GCE, and one and a half times at PMB/MWCNT/GCE.

The increased electrocatalytic activity and higher electron transfer rate mean that polymer/CNT composites are more suitable for electrochemical (bio) sensing than electrodes modified with only polymer.

3.1.2. Scan rate dependence for mechanistic studies

Cyclic voltammetry at different scan rates has been used at the polymer and polymer/CNT modified electrodes, to elucidate the redox reaction mechanisms.

PNR modified electrodes [7,52,72,105] exhibited a diffusion-controlled redox process, similar to other redox polymers: PMG, PMB [52], PBCB [40] and PBG [39]. However, there were some cases in which polymer-modified electrodes showed a linear dependence of peak current on scan rate, consistent with an adsorption-

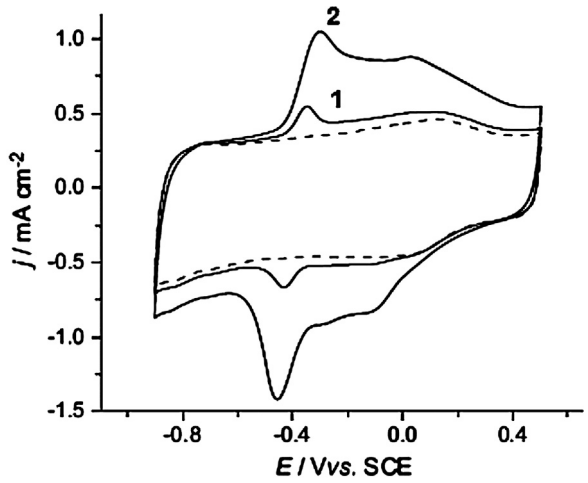

Fig. 9. Cyclic voltammograms at MWCNT/GCE (dashed line) and (a) MWCNT/PNB/GCE and (b) PNB/MWCNT/GCE; $v = 25$ mV s^{-1}. From [63], reproduced by permission of Elsevier.

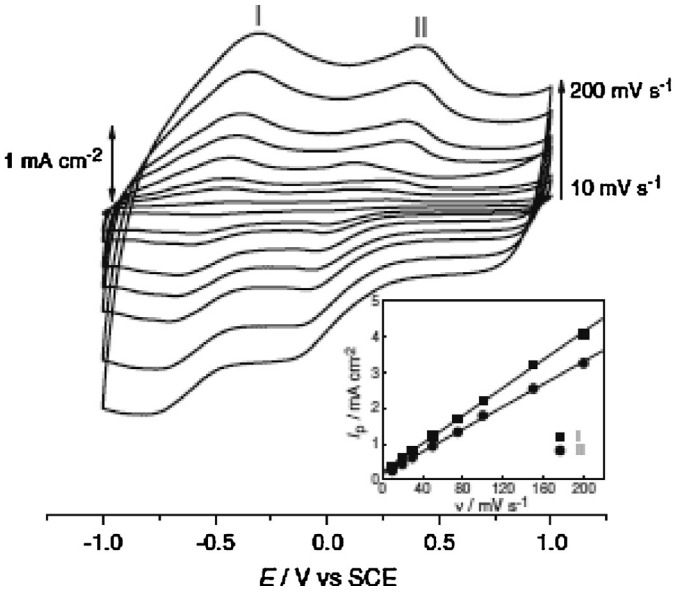

Fig. 10. CVs at PNR/MWCNT/GCE at different scan rates, v, between 10 and 200 mV s^{-1}; the inset is the plot of the anodic peak currents (I) and (II) vs. v. From [72], reproduced by permission of Springer.

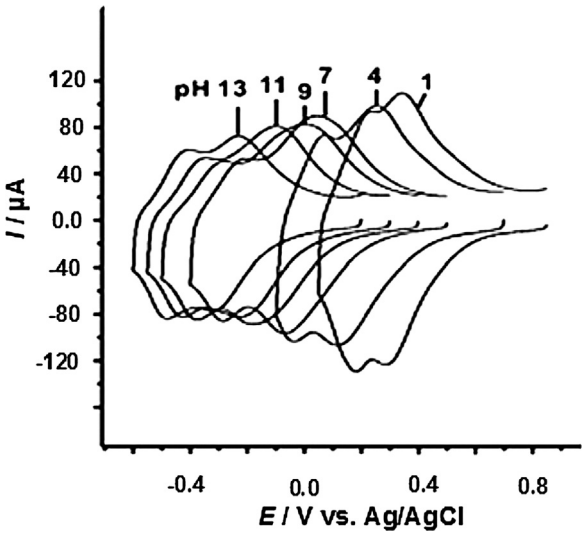

Fig. 11. CVs at of PMB/MWCNT/GCE in different pH; $E_{pa,c}$(mV) = 203–35 pH and $E_{1/2}$(mV) = 400–64 pH. From [49], reproduced by permission of Elsevier.

controlled process, e.g., PNB [106], PBCB [30,32], probably due to a more compact film structure, that is formed by potentiostatic deposition, e.g., [32] or by using a more concentrated monomer solution, e.g., [30], which hinders counterion diffusion through the film. With the inclusion of CNT, surface-confined electrochemical processes were found for PBCB [30,32,35], PMB [49–51], PMalG [41,42], PNB [61], PNR [72], PTBO [86] and PAB [93] (see Fig. 10), in some cases with very fast electron transfer kinetics [35].

Differences from the general behavior of polymer/CNT have been found for two polymers, for PNB [63] and PBG [39], for polymers being formed both beneath and on top of CNT. All these modified electrodes showed a diffusion-controlled electrochemical process with a more difficult diffusion occurring when PBG film was on top of CNT, explained by the compact structure of PBG film and by the fact that PBG can enter the porous structure of nanotubes, slowing diffusion [39].

In general, it can be concluded that the presence of only poly (phenazine) or poly(triphenylmethane) films on the electrode surface leads to a process controlled by the diffusion of counter ions into and out of the polymer film and when nanotubes are added, the process controlling the redox reaction is changed into a surface-confined one. Exceptions from this behavior might be due to different polymer structure/thickness, and CNT characteristics, as well as the CNT dispersion matrix.

3.1.3. Influence of pH

The electrochemical behavior of all polymer dye films reviewed here tends to be affected by the pH [107]. Studies of variation of response with pH were performed in different pH ranges, [32,35,37,38,41,42,49,75,87]. In all cases, the polymer redox peaks shifted linearly in the negative direction with increase in pH. The slope of the plot of peak potential vs. pH together with the peak width can give information about the number of electrons and protons transferred in the reaction. Different behaviors have been observed.

The slope values were close to the Nernstian value of −59 mV pH^{-1}, signifying an equal number of protons and electrons involved in the electrochemical process for the following electrode configurations: PTH/MWCNT [75], PMalG/MWCNT [41], PBG/MWCNT [38], PBCB/MWCNT [35,37], as also observed for PNR, PMB, PMG and PBCB [40,52]. On the other hand, slope values close to −30 mV pH^{-1}, correspond to an electron to proton ratio of 2, e.g., transfer of two electrons, coupled with one proton. This was the case of PMalG/MWCNT [42] and PBCB/SWNH [32]. The midpoint potential vs. pH plot of PMB/MWCNT exhibited two slopes, −63 mV pH^{-1}, for pH 1–7 and −35 mV pH^{-1}, for pH 7–13 (see Fig. 11), which corresponds to different reaction mechanisms [49].

3.1.4. Stability

The stability of the polymer and polymer/nanotube films deposited on various electrode substrates has been investigated, usually by cyclic voltammetry.

The rate of degradation of PBCB at GCE has been estimated by cyclic voltammetric scans at 50 mV s^{-1}, after 50 scans the oxidation/reduction currents decreasing by 11% and 7%, at pH 4.1 and 7.0, respectively [40]. The stability of the PBG film at CFE and MWCNT/CFE was examined by performing 30 or 100 scans in pH 7.0 buffer solution, the current decreasing by 7% and 23% for the oxidation and reduction processes, respectively [38,39].

High stability has been reported for PMalG/MWCNT/GCE in the pH range between 1 and 13 [41,44] and for PNB/SWCNT/GCE, which maintained the initial current after 50 cycles [61].

A comparison between the stability of polymer/CNT modified electrodes was made in [42,49]. The percentages of degradation of PMalG and PMalG/MWCNT were calculated after 280 min of cycling in H_2SO_4 pH 1.5 [42], PMalG/MWCNT decreasing by 12% and reaching a constant current after 200 min, while for PMalG the current decreases by 48% and continues to degrade on further cycling. In a similar manner, after continuous cycling for 300 min the amount of degradation for PMB/MWCNT and PMB at GCE was calculated to be 17 and 22%, respectively [49]. A comparison was done between BCB/SWCNT (adsorbed monomer) and PBCB/MWCNT and after 100 cycles the current corresponding to PBCB/SWCNT/GCE maintained 90% of the initial value, while that of BCB/SWCNT/GCE decreased by 53% after only 50 cycles, due to the additional covalent cross-linking of the bridged nitrogen atoms between CNT and PBCB, in addition to the π–π stacking that occurs between BCB and CNT [32].

Similar enhancements in CNT/polymer properties compared with CNT or polymer alone have been reported in the literature [108–110], leading to the conclusion that the presence of nanotubes greatly increases the stability of the polymer films.

3.2. Electrochemical impedance spectroscopy (EIS)

Electrochemical impedance spectroscopy (EIS) can give information on the impedance changes at the electrode surface during the modification process [111]. By providing data about the electron transfer resistance as well as about diffusion, EIS can offer valuable information about whether a modified electrode platform can enhance the rate of electron transfer. Various nanostructured modified electrodes with poly(phenazines) and poly(triphenylmethanes) in combination with carbon nanotubes have been analysed by EIS in the presence or absence of redox probe. Some of the results obtained will be discussed below, mainly in terms of charge transfer resistance.

Impedance spectra were recorded in the presence of the model electroactive species, $Fe(CN)_6^{3-/4-}$, in solution, for GCE modified with MWCNT and PNR, PBCB [31], PNR alone or together with FAD [70], PTH [77,81], PTBO [86], PMalG [44], as well as for PBCB/SWCNT modified electrodes [30]. Spectra of PNR or PBCB MWCNT/GCE modified electrodes in different configurations are shown in Fig. 12 [31]. Nearly all spectra had a similar shape, as expected in the presence of a redox probe, in the complex plane plot having a semicircle in the high frequency region due to the charge transfer process and a linear part in the low frequency region, due to diffusion control. The values of the charge transfer resistance, R_{ct}, were lower at CNT-modified electrodes than at the bare electrode, indicating that nanotubes improve the reaction rate, and they decreased further in the presence of polymers, except for PNR/MWCNT, where the charge transfer became more difficult. The lowest value was obtained for MWCNT/PBCB, and for MWCNT/PNR and PBCB/MWCNT the values are very similar.

In another configuration consisting in GCE modified with PNR, MWCNT and PNR/MWCNT [70], the spectra in the presence of $Fe(CN)_6^{3-/4-}$ also showed easier electron transfer for the electrode modified with both polymer and carbon nanotubes. Similar results were obtained for modified electrode architectures on GCE containing CNT together with PTH [77,81], PMalG, [44] and PBCB [30]. This may be attributed to the more effective deposition of the polymer film on CNT/GCE and to an increase in porosity of the accessible modified electrode surface, which increases the active sites where faradaic reactions can occur [44].

The higher value of R_{ct} for MWCNT/PNR-FAD/GCE compared to PNR-FAD/MWCNT/GCE, indicates a better electrode architecture with polymer on top [70].

Spectra with only the diffusional linear part were observed at PTBO and PTBO/MWCNT modified GCE, the diffusion of redox probe being the rate determining step over the whole frequency range and hindered due to the ultrathin films [86].

EIS experiments were performed in the absence of redox probe at PNB/MWCNT/GCE [63], PMB/MWCNT/CCE [50] and PBG/MWCNT/CFE [38,39]. In order to enable comparison, only spectra recorded at 0.0 V applied potential are taken into account, being common in all studies. In the absence of redox probe, a small or no semicircle appears in the high frequency region and there are diffusive lines for intermediate to high frequencies. The circuits used to fit these spectra generally include the cell resistance in series with a parallel combination corresponding to the capacitance and resistance of the modifier film, plus a diffusional Warburg element [39,50,63]. Following modification with PNB/MWCNT [63], the spectra showed a typical shape usually obtained for CNT: lines with two different angles: at high frequencies around 45° and at low frequencies close to 90°, the latter attributed to finite Warburg diffusion; at these electrodes the impedance values were in the sequence: MWCNT/GCE > MWCNT/PNB/GCE > PNB/MWCNT/GCE. Similar spectra were also exhibited by CFE modified with MWCNT, MWCNT/PBG and PBG/MWCNT [39]. However, at PBG/CFE the spectra showed a semicircle in the high frequency region with straight lines at low frequencies. These results clearly show that the overall electrical properties of the composite electrodes are more influenced by CNT than by the presence of the redox polymer.

The diffusion resistance calculated from the Warburg element was lower when CNT and polymer are present and in most cases was the lowest with polymer on top [38,63].

In the structures that have polymer together with CNT, the film resistance decreases and the capacitance values increase, compared with the polymer-only modified electrode, showing that the combination of nanotubes with polymer increases the electronic conductivity [50].

It can be concluded that the combination of poly(phenazine) and poly(triphenylmethane) polymers and nanotubes greatly

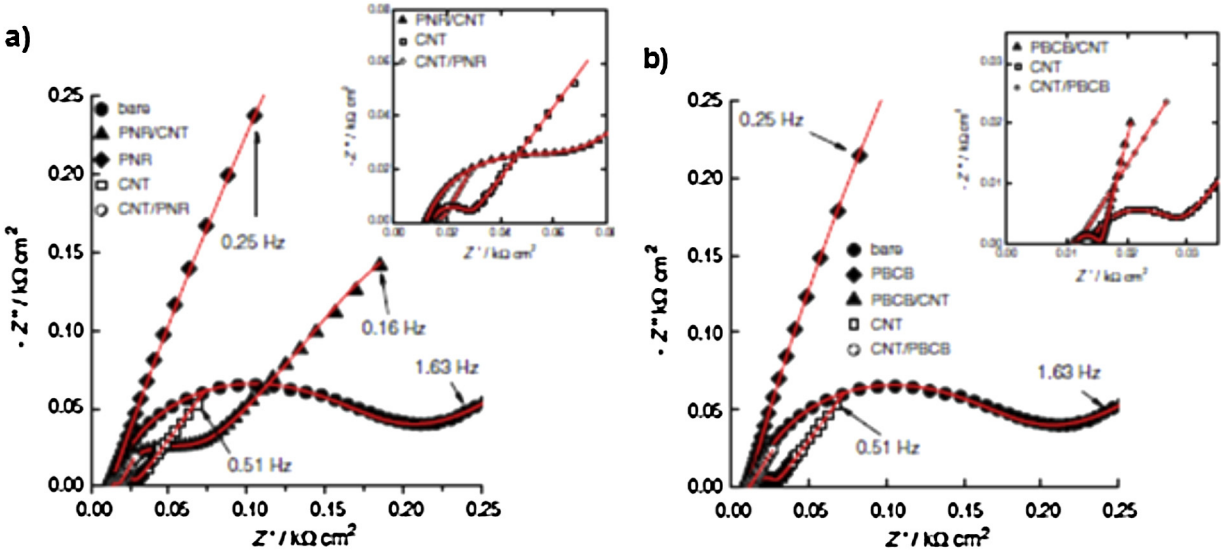

Fig. 12. Complex plane impedance spectra in 3 mM $K_3Fe(CN)_6$ + 0.1 M KCl at 0.15 V vs. SCE at different stages of modified electrode assembly for (a) PNR + MWCNT and (b) PBCB + MWCNT modified electrodes. The magnified insets show the spectra of only MWCNT and their combination with polymers. Lines show equivalent circuit fitting. From [31], reproduced by permission of Springer.

decreases the value of charge transfer resistance and increases the electronic conductivity of the modified electrodes.

3.3. Scanning electron microscopy (SEM)

Scanning electron microscopy (SEM) images can provide valuable information concerning the electrode surface morphology. Various poly(phenazine)/CNT and poly(triphenylmethane)/CNT structures prepared on different electrode substrates have been characterized by SEM.

Some SEM studies focus solely on the differences in the images of CNT before and after polymerization on top of them [37,49,79,81,85,86], while in a few others the polymers were present beneath the CNT [31,89]. The changes that occur in the poly (phenazine) morphology after their deposition on top of CNT are described in [7,45], and the differences that appear in polymer-CNT images compared with CNT or polymer only in [36,38,41,72]. A more detailed investigation, including a morphological study of the substrate where the polymer, nanotubes and their combination were immobilized was performed on GCE [47,79,81,86,89,95], ITO [31,36,38,41,72] and screen printed carbon electrodes (SPCE) [45]. The results obtained are shown in Figs. 13 and 14 and are discussed below.

The typical morphology of carbon nanotubes, both MWCNT and SWCNT, was very similar [36,38,41,72]. Most of the SEM images show the well-known small bundles [112], as seen in Fig. 14b_1–b_3, which are formed when large quantities of CNT are immobilized on GCE or ITO electrode surfaces [7,31,37,72,79,86]. The nanotubes appear to be highly dispersed [36,47,49] and homogeneously distributed [36,37,41,49,85,95] (Fig. 14b_4), as

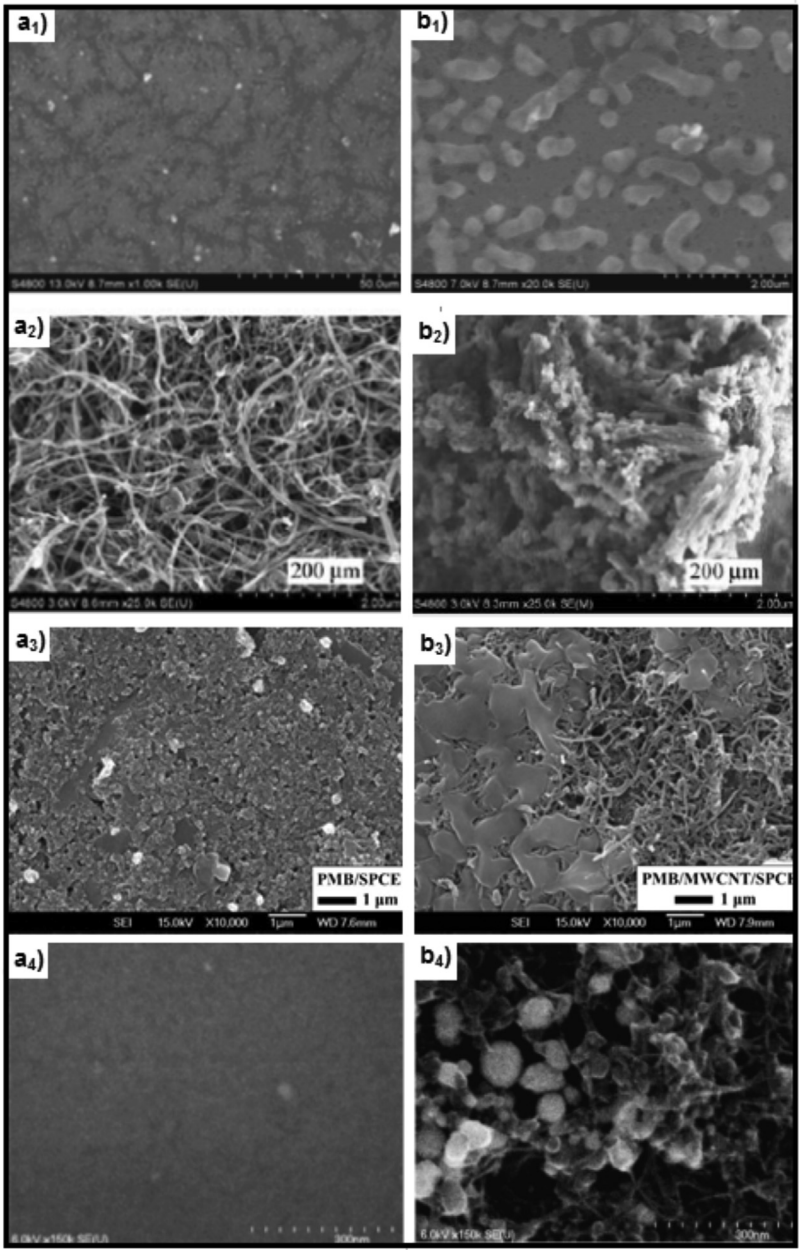

Fig. 13. SEM micrographs of (a_1) SWCNT/PTBO/GCE and (b_1) magnification of a_1: from [89], reproduced by permission of Springer; (a_2) thin and (b_2) thick film PTH/MWCNT/GCE: from [81], reproduced by permission of Wiley; (a_3) PMB/SPCE and (b_3) PMB/MWCNT/SPCE: from [45], reproduced by permission of Elsevier; (a_4) PPS/GCE and (b_4) PPS/SWCNT/GCE: from [95], reproduced by permission of Elsevier.

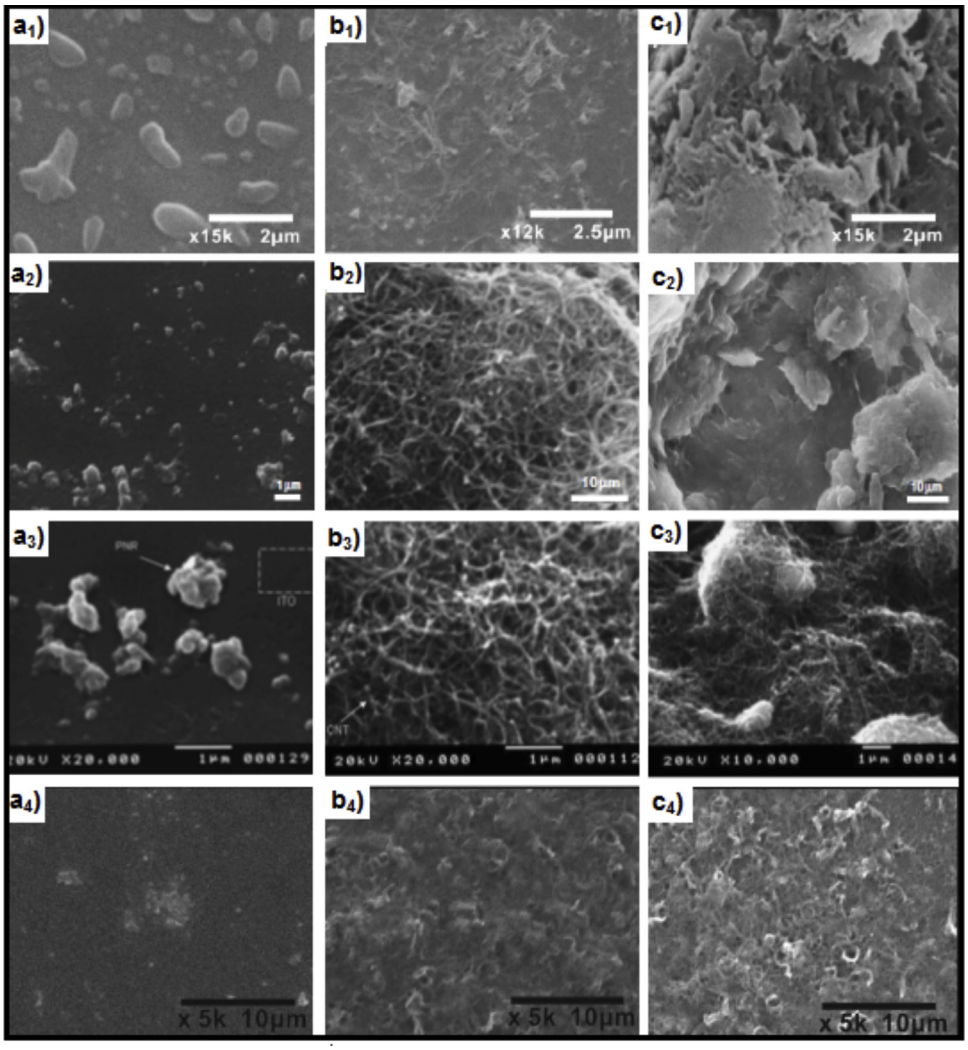

Fig. 14. SEM images of ITO electrodes modified with (a_1) PMalG, (b_1) MWCNT, (c_1) MWCNT/PMalG: from [41], reproduced by permission of Elsevier; (a_2) PBG, (b_2) MWCNT, (c_2) PBG/MWCNT: from [38], reproduced by permission of Springer; (a_3) PNR, (b_3) MWCNT, (c_3) PNR/MWCNT: from [72], reproduced by permission of Springer; (a_4) PBCB, (b_4) MWCNT and (c_4) PBCB/MWCNT: from [36], reproduced by permission of The Electrochemical Society.

reported also by [113], but individual nanotubes, disordered and entangling with each other, have been also observed [81,95] and a porous structure with 50–200 nm pores is mentioned [85].

Poly(phenazines), formed on bare electrodes, generally tend to form bunches on the electrode surface. PBG constitutes aggregates [38], Fig. 14a_2, and PNR tends to agglomerate [72], Fig. 14a_3, or to form a fibrous structure when deposited potentiostatically [7], while PMalG in Nafion® shows elongated beads [41], Fig. 14a_1. In some cases, no morphological differences can be distinguished from the SEM images of polymer modified electrodes compared to the bare electrodes, such as for PBCB on ITO [36] (Fig. 14a_4) and PPS on GCE [95] (Fig. 13a_4), which indicates the formation of very thin films. In [45] the authors report that PMB only adsorbed on some specific sites of the SPCE and the PMB formed does not cover the whole SPCE surface, Fig. 13b_3.

The electropolymerization of phenazines on the surface of CNT did not change the overall morphology, but made a more compact structure [37,79]. For PTBO/MWCNT nanowires, and PTH/MWCNT modified GCE, a special three-dimensional structure is reported, as observed in Fig. 13b_1 and a_2, [79,86], consisting of small bundles and single nanotubes, also visible for PNR/MWCNT/ITO, Fig. 14c_3. A three-dimensional structure of PPS/SWCNT is also observed with the formation of small and inhomogeneous polymer aggregates of 30–90 nm on the surface of the SWCNT [95], Fig. 13b_4. Poly (thionine) on top of MWCNT also forms aggregates, Fig. 13a_2, which overlap when a thicker polymer layer is deposited [81], Fig. 13b_2. PMB films stack on MWCNT and result in a porous structure [45] (Fig. 13b_3), similar to that formed by PMalG and PBG over MWCNT on ITO, as shown in Fig. 14c_1 and c_2 [41], also observed at PBCB/MWCNT and PNR/MWCNT [31]. Alternatively, polymer can also form clusters, as clearly shown in Fig. 14c_4 for PBCB over MWCNT on ITO electrodes [36]. By scanning tunneling microscopy, STM, with a higher magnification than SEM, it was possible to see the formation of nanometre-sized grains in between PMalG beads which revealed the coexistence of MWCNT and PMalG in the composite film [41].

When nanotubes are placed on top of PBCB and PNR, a similar network-like structure is observed, MWCNT/PNR being a more compact composite [31]. In other configurations with PTBO polymer covering SWCNT, a dendritic-like morphology was revealed (Fig. 13a_1), containing quite regular substructures of submicron size [89] (Fig. 13b_2).

Polymer formation on top of nanotubes is not always visible, as is the case of PMB on MWCNT/SPCE, Fig. 13b_3. However, a clear indication of polymer deposition is the slight increase in nanotube diameters, as reported in [79,85,86], meaning that the polymer layer is rather thin.

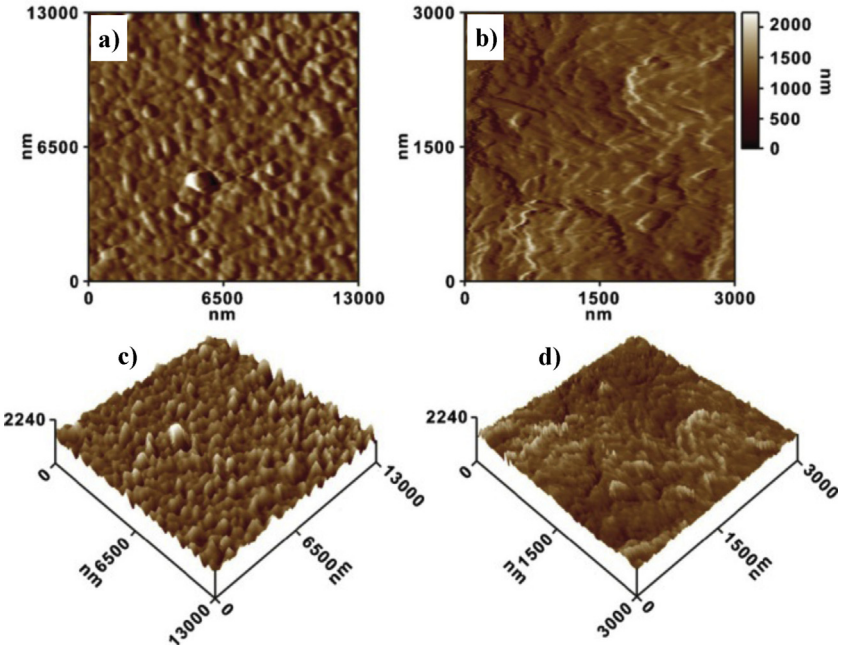

Fig. 15. AFM and 3D images of PNR (a and c) and PNR/MWCNT composite films (b and d). From [7], reproduced by permission of Elsevier.

3.4. Atomic force microscopy (AFM)

PNR and PNR/MWCNT synthesized on ITO by potentiostatic methods were characterized by AFM [7]. The topographic images obtained for PNR, Fig. 15a and c, show that PNR forms globular and fibrous structures, as also seen by SEM. On a larger scale, similar to that used for PNR, the surface of PNR/MWCNT was uneven so that the scale was reduced to ensure a more evenly scanned surface, Fig. 15b and d, clear differences being noticeable between PNR and PNR/MWCNT.

AFM images of the surface of the PPS and PPS-SWCNT modified GCE [95] show that the surface morphology is characterized by nodular structures typical of conducting polymers [114]. The thickness of the composite film is estimated to be 50–200 Å.

A magnified view of the PBCB, MWCNT and PBCB/MWCNT films on ITO by AFM reveals morphological differences between them, PBCB forming beads on ITO while PBCB/MWCNT presents an uneven surface [36]. The thicknesses of PBCB, MWCNT and PBCB/MWCNT films were estimated to be 231, 869, and 1700 nm respectively, demonstrating that the thicker film is PBCB/MWCNT.

The PBCB/GCE, SWCNT/GCE and PBCB/SWCNT/GCE assemblies have been characterized using AFM [30], the morphological differences between them being very clearly seen in Fig. 16. While the PBCB film is uniform, smooth and compact on bare GCE, Fig. 16a, the SWCNT/GCE surface is porous and reticulated. With PBCB on top of SWCNT, Fig. 16c, an increase in the diameter of the carbon nanotubes was observed, indicating that PBCB coated the SWCNT. A small amount of PBCB was deposited on GCE, the monomer polymerizing preferentially on CNT, interconnected PBCB-SWCNT networks being formed on the electrode.

Significant morphological differences between MWCNT, PMalG, and PMalG/MWCNT modified ITO electrodes were also observed [42]. The images reveal the presence of MWCNT clusters, smaller beads in the case of PMalG, while PMalG/MWCNT shows big arrangements of PMG covering MWCNT, making them less visible. The thicknesses of MWCNT, PMalG, and PMalG/MWCNT obtained using AFM were 350, 180, and 900 nm, respectively, consistent with the surface coverage values.

3.5. UV–vis spectroscopy

The interaction between polymers and CNT has been explored by UV–vis spectroscopy. The nanotube spectrum exhibits a featureless absorption [34,62,86,92,95], while that for monomers in aqueous solution displays a strong absorbance at 630 nm for TBO [86], 519 nm for PhS [95], 633 nm and 289 nm for azure-A [92], 637 nm for NB [62], 579 nm and 631 nm for BCB [34]. These spectra have also been observed in other studies with phenazines [86,115–117]. When mixing nanotubes with different monomers, different behaviors have been observed. For TBO, the absorption band shifted from

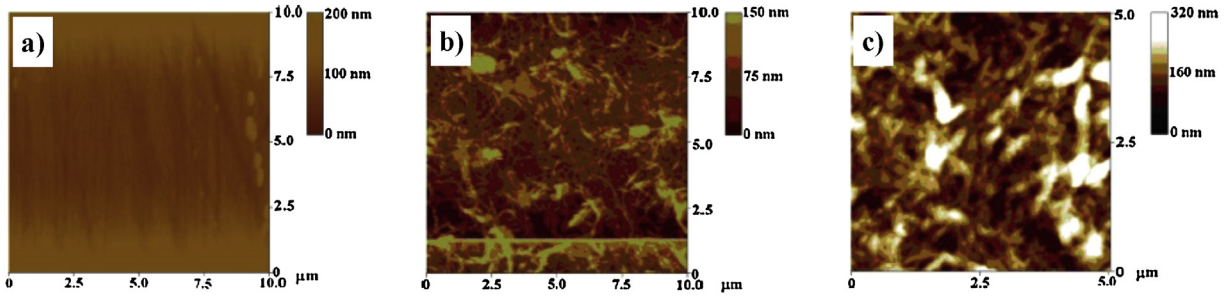

Fig. 16. AFM images of (a) PBCB/GCE, (b) SWCNT/GCE and (c) PBCB/SWCNT/GCE. From [30], reproduced by permission of Elsevier.

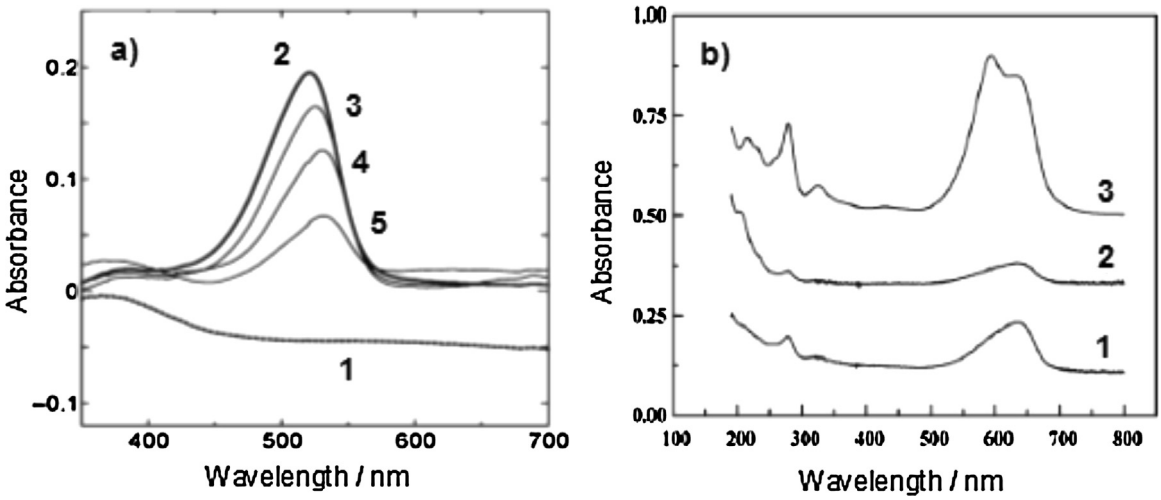

Fig. 17. Absorption spectra of (a) a-SWCNT suspension solution, b-PS solution and c–e-PS/SWCNT: c-10, d-25, and e-50 μg SWCNT: from [95], reproduced by permission of Elsevier; (b) a-NB monomer, b-NB/SWCNT and c-PNB/SWCNT: from [62], reproduced by permission of Elsevier.

630 nm to 610 nm [86] and two new peaks appeared at about 550 nm and 740 nm, respectively, due to aggregation of TBO molecules onto the MWCNT [115]. In the case of PS, the peak was red-shifted and the absorbance decreased when adding SWCNT in solution, due to PS adsorption onto the SWCNT through electronic interaction, the SWCNT acting as electron donors while PS molecules as acceptors [95,118], see Fig. 17.

In a similar way, the absorption peaks of azure-A were shifted to 621 nm and 275 nm, respectively, after adsorption onto CNT, attributed to the aggregation of azure-A molecules on the CNT [115]. For PNB on the surface of SWCNT, an additional absorbance peak is observed at 594 nm, see Fig. 17b, ascribed to the absorbance of PNB [66], while that at 637 nm, corresponding to NB monomer units inside the PNB structure, is maintained [62]. A slight red shift in the absorption peaks of BCB has also been observed [34], due to possible electrostatic, π–π, and dipole-dipole interactions [116].

4. Applications of poly(phenazine)/CNT and poly (triphenylmethane)/CNT modified electrodes as sensors and biosensors

This section will review the main analytical applications of redox polymer/CNT modified electrodes in sensors and biosensors, according to the analyte to be determined.

4.1. Glucose

Glucose is one of the most important analytes which can be measured by the polymer/CNT modified electrodes reviewed here, when covered by an enzymatic layer, i.e., a glucose biosensor. Glucose oxidase (GOx) is one of the most utilized enzymes, due to its low cost and robustness, and hence GOx based biosensors are the preferred tool to evaluate the performances of newly developed electrode biosensor platforms [119,120]. Glucose-based biofuel cells, in which glucose is oxidized at a GOx or glucose dehydrogenase (GlcDH) based anode, are also being investigated, with the aim of future implants to furnish an autonomous energy supply for medical grafts [121].

Glucose biosensors have been developed incorporating CNT/polyphenazine, both monoenzymatic, based on either GOx or GlcDH, and bienzymatic, immobilising horseradish peroxidase (HRP) together with GOx. The analytical properties of such biosensors are summarized in Table 2, and the biosensor mechanism in Fig. 18. The mechanism is based on either (A) detection of peroxide formed in the GOx enzymatic reaction, when O_2 acts as electron acceptor from $FADH_2$ or (B) direct regeneration of FAD at the polyphenazine mediator. Note that in route A, HRP is not always required for H_2O_2 detection.

Table 2
Biosensors and sensors based on CNT together with polyphenazines or polytriphenylmethanes.

Analyte	Electrode architecture	Technique	Media	LD/μM	Sensitivity/ $\mu A\,cm^{-2}\,mM^{-1}$	Linear range/mM	Reference
Glucose	Nano-$CaCO_3$-GOx-HRP/PBCB/SWCNT/GCE	Amp. −0.25 V[(a)]	PBS pH 6.5	1.0	42.3	$2.5e^{-3}$–3.0	[30]
	GlcDH-[1]C8-LPEI-PMG/CNTpaper	Amp. +0.3 V[(a)]	PBS pH 7.4		17.0*	5.0	[54]
	GlcDH/PNb–SWCNT/GCE	Amp. 0.05 V[(a)]	PBS pH 8.5	5.0	14.1	0.1–8.5	[61]
	GOx-$chit^+$/$MWCNT^-$/PNR-Nafion®$^+$/GCE		PBS pH 7.0	1.0		$5.0e^{-3}$–2.0	[4]
	GOx/MWCNT/PBCB/GCE	Amp. −0.3 V[(a)]	PBS pH 7.0	11.0	36.3	1.6	[31]
	GOx/PBCB/MWCNT/GCE			14.0	10.1	1.6	
	GOx/MWCNT/PPBR/GCE			20.0	2.7	1.3	
	GOx/PNR/MWCNT/GCE			17.0	30.4	1.6	
	GOx/$\{MWCNT/PNR\}_5$/GCE	Amp. −0.2 V[(a)]	PBS pH 7.0	10.0	5.33	0.05–10	[68]
	GOx/PTBO/MWCNT/GCE	Amp. −0.1 V[(b)]	PBS pH 7.4	–	14.5	1.0–7.0	[83]
	GOx + HRP/PTBO/MWCNT/GCE	Amp. −0.1 V[(b)]	PBS pH 7.4	30.0	113.0	0.1–1.2	[84]
Ethanol	AlcDH/PBCB/SWCNT/GCE	Amp. 0.0 V[(a)]	PBS 7.5	100	71.42*	0.4–2.4	[32]
	PMalG/Nafion®/MWCNT/GCE	DPV 0.58 V[(b)]	[2]KHP pH 4.0	100	3.8	3.1–72.5	[41]
	AlcDH/PNb-SWCNT/GCE	Amp. +0.1 V[(a)]	PBS pH 8.3	50	94.4	0.1–3.0	[62]
Sorbitol	[3]DSDH/PMG/MWCNT/GCE	Amp. +0.2 V [(a)]	Tris–HCl pH 9.0	110	8.7	0.2–1.2	[58]

Table 2 (*Continued*)

Analyte	Electrode architecture	Technique	Media	LD/μM	Sensitivity/ $\mu A\,cm^{-2}\,mM^{-1}$	Linear range/mM	Reference
	DSDH/PMG/MWCNT/GCE	Amp. +0.2 V [b]	Tris-HCl pH 9.0	100	-	0.1–4.5	[59]
NADH	PMB/MWCNT/[4]SPCE	Amp. +0.2 V[b]	PBS pH 7.0	1.0	26.3	$1.0e^{-3}$–1.0	[45]
	[1]C8-LPEI-PMG/CNTpaper	Amp. +0.3 V[a]	PBS pH 7.4		243*		[54]
	PBCB/SWCNT/GCE	Amp. 0.0 V[a]	PBS pH 7.5	1.0	10.0*	$3.0e^{-3}$–0.1	[32]
	PTH/MWCNT/[5]CILE	Amp. 0.0[b]	PBS pH 7.0	0.26	151	$0.8e^{-3}$–0.4	[75]
	PTBO/MWCNT/GCE	Amp. 0.0[a]	PBS pH 7.0	0.5	130	$2.0e^{-3}$–4.5	[86]
	PPhS/SWCNT/[6]EPPG	Amp. 0.0[b]	PBS pH 7.0	0.01	576	0.2	[95]
	PNR-FAD/MWCNT/GCE	Amp. 0.1[b]	PBS pH 7.0	1.3	457.2	$1.3e^{-3}$–0.9	[70]
	PTBO/MWCNT/GCE	Amp. 0.05[b]	PBS pH 6.0	*	500	0.0–2.0	[60]
	PMG/MWCNT/GCE				350	0.0–2.5	
	PAB/MWCNT/GCE	Amp. 0.1[b]	PBS pH 7.4	0.07	4.0	$0.2e^{-3}$–0.7	[93]
	PAA/MWCNT/GCE	Amp. 0.14[b]	PBS pH 7.4	0.2	–	$0.6e^{-3}$–0.6	
	PTH/MWCNT/GCE	Amp. 0.20[b]	PBS 7.4	0.2	–	$0.7e^{-3}$–0.7	
	PNR/f-MWCNT/GCE comp1	CV 0.1 V[b]	PBS 6.0	–	–	1.5 mM	[69]
	PNR/f-MWCNT/GCE comp2	CV 0.15 V[b]		–		1.5 mM	
H_2O_2	HRP/PTBO/CNT/GCE	Amp. −0.1 V[b]	PBS pH 7.4	20.0	604.0	0.02–0.4	[84]
	PBCB/SWCNT/GCE	Amp. −0.3 V[a]	PBS pH 7.0	0.12	57.7	$0.5e^{-3}$–0.2	[33]
	Nano-$CaCO_3$-HRP/PBCB/SWCNT/GCE	Amp. −0.25 V[a]	PBS pH 6.5	1.0	15.5	$5.0e^{-3}$–1.2	[30]
	CNT/PBG/[7]CFE	Amp. 0.0 V[a]	PBS pH 7.0	0.91	152	$0.5e^{-3}$–6.0	[39]
	PBG/CNT/CFE	Amp. 0.0 V[a]	PBS pH 7.0	1.45	114	$0.5e^{-3}$–6.0	
	MWCNT/PMB/[8]CCE	Amp. 0.0 V[a]	KCl + HCl	20.7	108	0.1–0.3	[50]
	PNR-FAD/MWCNT	Amp. −0.2 V[b]	PBS pH 7.0	0.1	10.1	$1.0e^{-3}$–2.6	[70]
	HRP/PtNP-PNR/MWCNT/GCE	Amp. −0.22 V[a]	PBS pH 7.0	1.1	35.0	$3.6e^{-3}$–4.3	[71]
	PTBO/ZrO_2/MWCNT/GCE	Amp. −0.15 V[b]	PBS pH 7.0	*	$82.1e^3$	0.05–0.3	[92]
	HRP/MWCNT-AuNPt/PTH/GCE	Amp. +0.4 V[a]	PBS pH 7.0	3.0	66.7	$5.0e^{-3}$–7.0	[74]
Ascorbate	PNR/MWCNT/GCE	Amp. 0.05 V[a]	PBS pH 5.5	4.7	375	0.8	[72]
	PNR/MWCNT/GCE	DPV 0.25 V[b]	[7]KHP pH 4.0		28*	0.08–0.2	[7]
	PNB/MWCNT/GCE	Amp. 0.0 V[a]	PBS pH 5.3	2.4	857	0.01–0.1	[63]
	PMB/MWCNT/GCE	CV 0.08 V[b]	PBS pH 7.4	200	11.3	$2.5e^{-3}$–0.8	[49]
	PMalG/MWCNT/GCE	DPV -0.02 V[b]	PBS pH 7.0	0.23	$20.4\ e^3$	$0.4e^{-3}$–0.1	[44]
	PBG/MWCNT/CFE	Amp. 0.0 V[a]	PBS pH 7.0	2.4	161.0	0.2	[38]
Nitrite	PAA/SWCNT/GCE	Amp. 0.1 V[a]	0.2 M H_2SO_4	1.0	240.0	$3.0e^{-3}$–4.5	[92]
	SWCNT/PTBO/GCE	Amp. 0.92 V[b]	PBS pH 7.0	0.37	84.3	$1.0e^{-3}$–4.0	[89]
	PTH/CNT/GCE	Amp. 0.0 V[a]	0.5 M H_2SO_4	1.4	5.81*	50	[76]
	PMB/MWCNT-CILE	Amp. 0.77 V[b]	PBS pH 4.0	0.25	$2.5\ e^3$	0.5–$68.0e^{-3}$	[46]
DA	PBG/MWCNT/CFE	DPV 0.15 V[a]	PBS pH 7.0	1.60	1200	$5.0e^{-3}$–0.12	[38]
	PMB/MWCNT/GCE	CV 0.26 V[b]	PBS pH 7.4	67.0	22	$2.5\ e^{-3}$–0.8	[49]
	PNR/f-MWCNT/GCE	DPV 0.35 V[b]	KHP 4.0	–	146*	0.08–0.2	[7]
EP	PMalG/MWCNT/GCE	DPV 0.2 V[b]	PBS pH 7.0	0.08	6700	$0.1e^{-3}$–0.1	[44]
	PMB/MWCNT/GCE	CV 0.23 V[b]	PBS pH 7.4	69.6	12	$2.5\ e^{-3}$–0.8	[49]
	PNR/f-MWCNT/GCE-comp1	CV 0.35 V[b]	PBS 6.0	–	20.0*	1.5	[69]
	PNR/f-MWCNT/GCE-comp2	CV 0.35 V[b]		–	80.0*	1.0	
	PBCB-MWCNT/GCE	LSV	PBS 6.0	0.01		$0.05e^{-3}$–0.05	
UA	PMalG/MWCNT/GCE	DPV 0.38 V[b]	PBS pH 7.0	0.12	710	0.3–$90e^{-3}$	[44]
	PNR/f-MWCNT/GCE	DPV 0.52 V[b]	KHP 4.0	–	0.08*	0.08–0.2	[7]

* – unknown electrode area [a] vs. SCE; [b] vs. Ag/AgCl; [1]C8-LPEI – Octylmodifiedlinear poly(ethylenimine); [2]KHP – potassium hydrogen phthalate; [3]DSDH – D-sorbitol dehydrogenase; [4]SPCE – screen printed carbon paste electrode; [5]CILE – carbon nanotubes ionic liquid paste electrode; [6]EPPG – edge-plan pyrolytic graphite; [7]CFE – carbon film electrodes; [8]CCE – carbon composite electrodes.

Biosensors based on GOx were GCE modified with nano-$CaCO_3$-GOx-HRP/PBCB/SWCNT [30], GOx-chit$^+$/MWCNT$^-$/PNR-NF$^+$ [67], GOx/MWCNT/PBCB, GOx/PBCB/MWCNT, GOx/MWCNT/PPBR, GOx/PNR/MWCNT [31], GOx/{MWCNT/PNR}$_5$ [68], GOx/PTBO/MWCNT [83] and GOx + HRP/PTBO/MWCNT [84]. The highest sensitivity was of GOx + HRP/PTBO/MWCNT/GCE [84], 113 $\mu A\,cm^{-2}\,mM^{-1}$, operating at −0.1 V vs. Ag/AgCl, following the mechanism in Scheme 1. The authors found that the bienzyme electrode offered improved sensitivity compared with the MWCNT-based mediator-free bienzyme electrode utilizing Nafion® [122], due to competition between oxygen and oxidized mediator for the regeneration of enzyme cofactor. When no O_2 is dissolved in solution, the first path Scheme 1, (A) is eliminated, as also stated in [83] and [31]. Lowest detection limits of 1 μM were achieved by Nano-$CaCO_3$-GOx-HRP/PBCB/SWCNT/GCE [30] and GOx-chit$^+$/MWCNT$^-$/PNR-Nafion®$^+$/GCE [67]. In [31], comparing the four different biosensors, it was observed that the best biosensor configurations were GOx/MWCNT/PBCB/GCE and GOx/PNR/MWCNT/GCE.

GlcDH based biosensors, which are NADH or NADPH cofactor dependent, as shown in Fig. 19, were mainly developed to be used as bio-anodes in biofuel cells [45,51,54,55], excepting that in [61]. GlcDH bioanodes are listed in Table 3. In [55], MWCNT were integrated in buckeye paper (BEP), and PMG was used as an NADH catalyst, these nanostructured bio-anodes, BEP-PMG-GlcDH, being assembled in quasi-2D capillary driven flow systems for real fuel cell applications. The GlcDH-biobattery based on GlcDH/PMB/MWCNT/SPCE reported in [45] reached a maximum power density of 2.4 $\mu W\,cm^{-2}$, 10 times higher than GlcDH/PMB/SPCE without CNT, while Chit/GlcDH/PMB–single walled nano-horns (SWNH)/GCE [51], which operate as shown in Fig. 19, have 10.74 $\mu W\,cm^{-2}$.

In [54], PMG, the crosslinker and the enzymes were co-immobilized on a octylmodified-linear poly(ethylenimine)

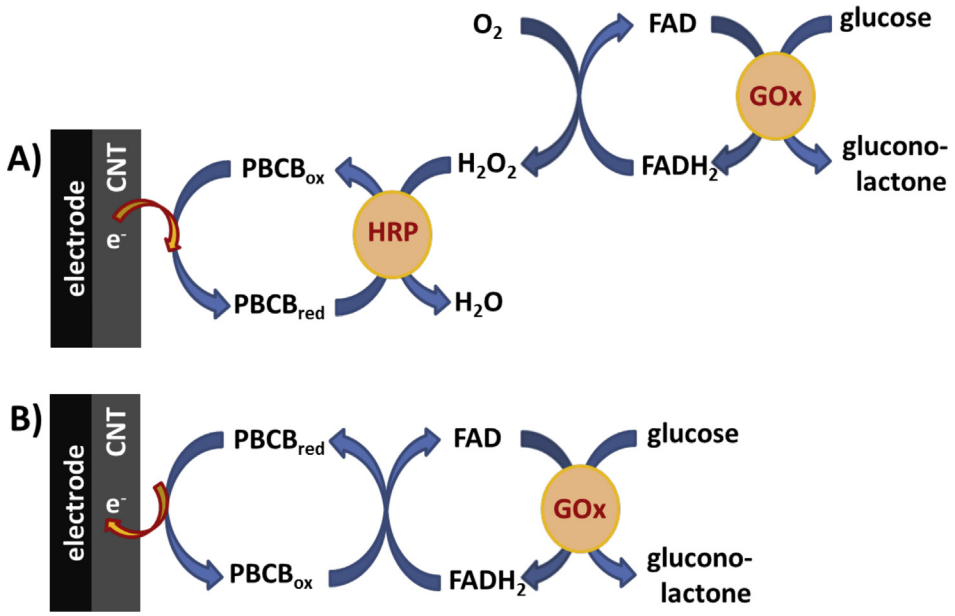

Fig. 18. GOx biosensor mechanism (A) in a bi-enzymatic configuration, when detection is based on the detection of peroxide formed in the first GOx enzymatic reaction and (B) based on the direct regeneration of FAD at polyphenazine mediator.

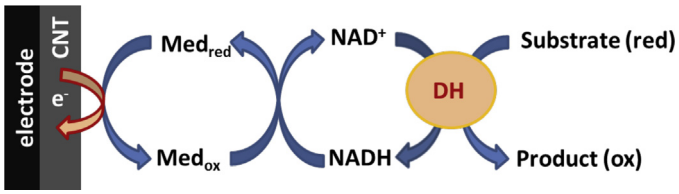

Fig. 19. Dehydrogenase enzyme (GlcDH, AlcDH, DSDH) biosensor mechanism based on NAD$^+$ regeneration at polyphenazine mediator.

(C8-LPEI) hydrogel on CNT paper substrate. The biosensor exhibited a sensitivity of 17.0 μA mM^{-1}, at +0.3 V, showing the applicability of these CNT papers for the fabrication of enzymatic bioanodes.

4.2. Ethanol

Ethanol has drawn attention as a biofuel since it can be produced by fermentation of biomass, its use in enzymatic fuel cells offering the possibility of small-scale power generators. For this purpose, many ethanol dehydrogenase based bioanodes have been reported and reviewed in [123].

A few CNT/polyphenazine based biosensors, all containing the NAD$^+$-dependent enzyme alcohol dehydrogenase (AlcDH) for the detection of ethanol have been reported, with the following configurations: AlcDH/PBCB/SWCNT/GCE [32], AlcDH/PNB-SWCNT/GCE [62], AlcDH/casting agent/MWCNT/PMG/carbon cloth, AlcDH/MWCNT/casting agent/PMG/carbon cloth, AlcDH/MWCNT/PPyr/PMG/carbon cloth, AlcDH/PPyr/MWCNT/PMG/carbon cloth [56], AlcDH/MWCNT/PMG/BEP [55]. A non-enzymatic sensor based on PMalG mediation, PMalG/Nafion®/MWCNT/GCE, has also been reported, which enabled the detection of three aliphatic alcohols, methanol, ethanol and propanol, by using DPV [41]. The sensor had a wide linear range up to 95.4, 72.5 and 49.0 mM for methanol, ethanol and propanol, respectively.

In [62], the role of MWCNT in the biosensor architecture was crucial, the AlcDH/PNB/GCE sensitivity being substantially lower than that of AlcDH/PNB-SWCNT/GCE. The authors also underlined the high operational stability of the electrode, which demonstrates a good resistance of the electrode to fouling, a common issue for the oxidation of NADH at solid electrodes.

AlcDH based CNT/polyphenazine bioanodes were all based on PMG mediation and are listed in Table 3. All followed the reaction mechanism presented in Fig. 19. In [56] several bioanode architectures constructed on carbon cloths (Ccl) were evaluated

Table 3
Bioanodes based on CNT/polyphenazine modified electrodes.

Analyte	Electrode architecture	Media	P/μW cm^{-2}	OCP/mV	I_{max}/μA cm^{-2}	Reference
Glucose	GlcDH/PMB/MWCNT/[1]SPCE	PBS pH 7.0	0.26	420	–	[45]
	GlcDH/PMB/SPCE		2.43	410		
	Chit/GlcDH/PMB–[2]SWNH/GCE	PBS pH 7.4	10.74	430	–	[51]
	GlcDH/MWCNT/PMG/[3]BEP	PBS pH 7.5	–	180	3382	[55]
Ethanol	AlcDH/MWCNT/PAMAM//PMG/[4]Ccl	PBS pH 7.4	278	459	–	[56]
	AlcDH/PAMAM/MWCNT/PMG/Ccl		189	356		
	AlcDH/MWCNT/Nafion®/PMG/Ccl		137	277		
	AlcDH/Nafion®/MWCNT/PMG/Ccl		32	149		
	AlcDH/MWCNT/PPyr/PMG/Ccl		24	224		
	AlcDH/PPyr/MWCNT/PMG/Ccl		29	186		
	AlcDH/MWCNT/PMG/Ccl		36	229		
	AlcDH/MWCNT/PMG/BEP	PBS 7.5	–	–	227	[55]

based on PMG and MWCNT together with two casting agents, poly (amido amine)dendrimer (PAMAM) and tetrabutylammonium modified-Nafion®, and the conducting polymer polypyrrole, in different configurations. The addition of MWCNT and casting agents improved bioanode performance, while polypyrrole decreased it. The position of both casting agents and MWCNT played a role in the bioanode response. The bioanodes with best performances were those containing PAMAM, the highest power densities, of 278 189 $\mu W\,cm^{-2}$, being achieved with the configuration AlcDH/MWCNT/PAMAM//PMG/Ccl.

In [55], besides AlcDh, GlcDH and lactate dehydrogenase (LDH) were also tested for the development of bioanodes, based on MWCNT and PMG immobilized on buckeye paper. Under similar conditions, the kinetic parameters obtained for GlcDH were superior to LDH and AlcDH, the GlcDH bioanode having j_{max} = 3.3 $mA\,cm^{-2}$, K_M = 17.5 mM compared to 226.6 $\mu A\,cm^{-2}$, K_M = 16.0 mM and 53.4 $\mu A\,cm^{-2}$ and K_M = 6.6 mM for AlcDH and LDH biosensors, respectively.

4.3. Sorbitol

Two biosensors for sorbitol detection have been developed and reported, based on the enzyme D-sorbitol dehydrogenase (DSDH) and on PMG mediation: DSDH/PMG/MWCNT/GCE [58] and DSDH/TEOS-PEI/PMG/MWCNT/GCE [59], both containing a porous silica film in which DSDH and NADH are co-immobilized, the difference being that the latter contained diaphorase to catalyze regeneration of the oxidized form of the cofactor, NAD^+. The biosensor mechanism is presented in Fig. 19.

In [58], the biosensor was first tested with NADH in solution, and it was observed that the role of PMG was essential, no response being recorded at MWCNT/GCE and only a small one at PMG/GCE, because of the lack of or poor electrocatalytic oxidation of NADH. Only the system including both MWCNT and PMG had a satisfactory sensitivity to D-sorbitol, due to synergetic effects of both MWCNT, which allowed an increased electroactive surface area, and PMG with catalytic properties toward NADH oxidation. A reagentless biosensor was then developed, by co-immobilizing the cofactor with the enzyme, the gel allowing NAD^+ to reach the catalytic site of the dehydrogenase, to perform oxidation of D-sorbitol, and was also able to interact with PMG/MWCNT/GCE to enable regeneration of NAD^+.

The biosensor based on PMG mediation developed in [59], only sensed sorbitol with NAD^+ in the solution, free-diffusing NADH generated by the immobilized dehydrogenase being able to be oxidized. A lack of biosensor activity after co-immobilizing the cofactor and the enzyme in the sol–gel was observed, this problem being overcome by using a flexible osmium complex mediator.

4.4. NADH

Electroanalytical applications of NAD^+-dependent dehydrogenases are based on electrochemical oxidation of the reduced cofactor (NADH) which is produced during the enzymatic reaction with the analyte to be determined. Development of effective systems for oxidation of NADH to enzymatically active NAD^+ is a critical step in the investigation of application of dehydrogenases in reagentless biosensors [124]. The direct oxidation of NADH at a conventional solid electrode surface is highly irreversible, takes place at high overpotentials, and usually involves the formation of radical intermediates that cause electrode fouling and the loss of analytical sensitivity, reproducibility and operational lifetime [125]. Among the many modified electrodes able to catalyze the oxidation of NADH at a low potential, special attention was paid to CNT/poly(phenazine) modified electrodes, which have been

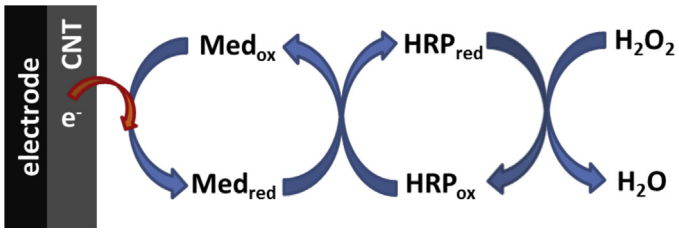

Fig. 20. Mechanism of hydrogen peroxide reduction at HRP/poly(phenazine)/CNT modified electrodes.

shown to present synergistic electrocatalytic effects for NADH oxidation [62]. The analytical parameters obtained at different carbon nanotubes/poly(phenazine) modified electrodes are shown in Table 2. Glassy carbon is, by far, the most used electrode substrate, but a carbon ionic liquid electrode, CILE [75], as well as a carbon nanotube paper electrode, CNTpaper [54], edge-plane pyrolytic graphite, EPPG [95], and a screen printed carbon electrode [45] have also been used. The CNT are mainly multi-walled, except those in [32,95], which are single-walled. PMG [54,58,60] is the most used redox mediator for NADH sensing, followed by PTH [75,93], PTBO [60,86] and PNR [69,70]. However, the most sensitive architecture involves) PPhS and SWCNT [95], which also exhibits the lowest detection limit.

4.5. Hydrogen peroxide

Hydrogen peroxide sensors are extremely important since H_2O_2 has great importance in pharmaceutical, clinical, environmental, mining, textile and food manufacturing applications, also being a product generated in biochemical reactions catalyzed by oxidase enzymes [126].

Its determination has been carried out using various polymer dye/CNT configurations with and without the enzyme horseradish peroxidase (HRP). The analytical parameters obtained at different electrodes are summarized in Table 2. Measurements without HRP have been performed mainly at glassy carbon electrodes modified with SWCNT and polymerized brilliant cresyl blue, PBCB/SWCNT/GCE [30], amino-functionalized MWCNT as a template to immobilize PNR and flavin adenine dinucleotide (FAD) [70], MWCNT and zirconia nanoparticles, on which poly(toluidine blue) was deposited, PTBO/ZrO_2/MWCNT/GCE [87], as well as carbon film electrodes modified with MWCNT and PBG [39]. Another configuration is based on the incorporation of MWCNT into a PMB film immobilized on carbon composite electrodes [50]. The highest sensitivity was obtained at PTBO/ZrO_2/GCMWCNT/GCE.

In [30] HRP was entrapped in a nano-$CaCO_3$ matrix followed by cross-linking with glutaraldehyde to give nano-$CaCO_3$-HRP/PBCB/SWCNT/GCE. This method is known to be simple, versatile and efficient, leading to sensitive and stable biosensors. The mechanism of this type of biosensor is represented in Fig. 20. Other enzymatic architectures include MWCNT, PNR and platinum nanoparticles, HRP/PtNPt-PNR/MWCNT/GCE [71], PTH and gold nanoparticles (AuNP), HRP/MWCNT-AuNPt/PTH/GCE [74] and in other work a bienzymatic architecture was developed with HRP together with glucose oxidase and PTBO, PTBO/MWCNT/GOx-HRP [84]. The highest sensitivity was achieved at PTBO/MWCNT/GOx-HRP and the lowest detection limit at Nano-$CaCO_3$-HRP/PBCB/SWCNT/GCE.

4.6. Ascorbate

Ascorbic acid/ascorbate is a vital component of the human diet. Ascorbate prevents scurvy and is known to take part in a number of

biological reactions. It is accepted to be the primary antioxidant in human blood plasma and is present in the mammalian brain together with various neurotransmitter amines including dopamine, epinephrine and norepinephrine [127]. Direct and selective detection of ascorbate at conventional or metal electrodes is difficult due to its large overpotential and electrode fouling by oxidation products [128].

Many strategies have been developed, using different types of modified electrode, to reduce the overpotential for the catalytic electrooxidation of ascorbate, among them carbon nanotube/polyphenazine modified electrodes, which are summarized in Table 2. All of them consist in GCE substrates modified with MWCNT, except one, which uses a carbon film electrode substrate [38], and the sensor platforms contain PNR [7,72], PNB [63], PMB [49], PMalG [44] or PBG [38] as redox mediator. The most sensitive was PMalG/MWCNT/GCE, which also exhibited the lowest detection limit, 0.23 μM [44].

4.7. Nitrite

Nitrites occur naturally in soil, in water, and in some foods, playing an important role in the environment. Being a toxic and a possible carcinogenic species [129], electrochemical sensors have been developed for its detection.

Four amperometric sensors have been reported for nitrite detection based on polyphenazines together with CNT, PAA/SWCNT/GCE [92], SWCNT/PTBO/GCE [89], PTH/CNT/GCE [76], and PMB/MWCNT-CILE [46].

In [92], a synergetic effect of PAA and CNT led to an improved sensor sensitivity at +0.1 V vs. SCE, higher than that of GCE modified with PAA or CNT alone, while the bare GCE showed no activity toward nitrite reduction. This is explained by an increased mass of PAA deposited on CNT/GCE and the fact that the PAA/CNT nanocomposite provides a large catalytic surface and facilitates electron transfer. The sensitivity of PAA/SWCNT/GCE, 240 $\mu A\,cm^{-2}\,mM^{-1}$, was higher than that of SWCNT/PTBO/GCE, 84.3 $\mu A\,cm^{-2}\,mM^{-1}$, which operated at a very positive potential of 0.92 V vs. Ag/AgCl. Better electrocatalytic behavior of SWCNT/PTBO/GCE compared to PTBO/GCE was reported, with a less negative nitrite reduction potential and an increase in sensitivity [89]. Of the four sensors, the highest sensitivity was that of PMB/MWCNT, being 2530 $\mu A\,cm^{-2}\,mM^{-1}$, at +0.77 V vs. Ag/AgCl, in which PMB was deposited on a CNT ionic liquid paste electrode. The presence of MWCNT in the carbon ionic liquid electrode composition, enhanced the surface coverage of PMB and decreased the degradation of PMB [46].

Depending on the applied potential applied in the amperometric studies, two reaction mechanisms are encountered, at PTBO and PTH-based sensors, respectively: $PTBO_{ox} + NO_2^- \rightarrow PTBO_{red} + NO_3^-$, followed by $PTBO_{red} \rightarrow PTBO_{ox} + 2e^- + 2H^+$ [89], or $PTH_{red} + NO_2^- \rightarrow PTH_{ox} + NO$, followed by $PTH_{ox} + 2e^- + 2H^+ \rightarrow PTH_{red}$ [76].

4.8. Dopamine

Dopamine (DA) is one of the most important neurotransmitters in the central nervous system of mammals, and which exists in the tissues and body fluids in the form of cations for controlling the nervous system [130]. Electrodes can sensitively detect the neurotransmitters which are present in living organisms [131]. However, since bare electrodes cannot distinguish between AA, EP and DA, due to their overlapping peaks, modified electrodes have been developed. Poly(phenazine)/CNT modified electrodes for dopamine sensing include glassy carbon modified with MWCNT on which poly(brilliant green) [38], poly(methylene blue) [49] or poly (neutral red) [7] has been deposited. The detection was performed by either CV [49] or DPV [7,38] and the most sensitive architecture was PBG/MWCNT/CFE [38].

4.9. Epinephrine

Epinephrine (EP) is a catecholamine neurotransmitter with an important role in human health. Electrochemical sensors are widely used but the oxidation products adsorb on bare electrodes, so that modified electrodes are needed [132].

Four poly(phenazine)/CNT sensor architectures have been used for EP determination, PMalG/MWCNT/GCE [44], MWCNT–PMB/GCE [49], PNR/MWCNT/GCE [69] and PBCB-MWCNT/GCE [37].

The electrochemical oxidation of epinephrine on PMalG/MWCNT/GCE was investigated in PBS ($5.0 \leq pH \leq 9.0$), the anodic peak currents reaching a maximum value at pH 7.0 with a gradually decrease with further increase of pH. Oxidation of EP occurred in a diffusion-controlled process, and chronoamperometry at 0.17 V vs. Ag/AgCl allowed the determination of EP's apparent diffusion coefficient, which was found to be $5.7 \times 10^{-6}\,cm^2\,s^{-1}$ [44]. PMalG/MWCNT/GCE permitted good separation between AA, EP and UA [44] as did MWCNT–PMB/GCE [49], the latter showing an enhanced electrocatalytic effect. EP was also determined at PNR/f-MWCNT/GCE [69]. However, the highest sensitivity was at PMalG/MWCNT/GCE [44], and the lowest detection limit was achieved by PBCB–MWCNT/GCE [37], as seen in Table 2.

4.10. Uric acid

Uric acid (UA) and other oxypurines are the principal final products of purine metabolism in the human body [133]. Abnormal levels of UA cause symptoms of several diseases, including gout, hyperuricemia and Lesch–Nyan disease [134]. In biological fluids, such as blood and urine, UA coexists with AA and DA. Electrochemical analysis at unmodified electrodes, for example glassy carbon, has limitations because of the overlapping of the oxidation potentials of AA, DA and UA and a pronounced fouling effect [135]. Among the modified electrodes developed for the determination of uric acid, poly(phenazine)/CNT with PNR [7] or PMalG [44] are examples. Both use DPV for determination of EP, in different media, pH 4.0 and 7.0. Linear ranges were up to 0.09 or 0.2 mM, and at PMalG/MWCNT/GCE the limit of detection was 0.3 μM.

4.11. DNA nucleobases

Deoxyribonucleic acid (DNA) encodes the genetic instructions while ribonucleic acid (RNA) performs multiple vital roles in the coding, decoding, regulation and expression of genes. Uracil is a pyrimidine base in RNA, playing an important role in biochemical processes which relate to several diseases and metabolic disorders [136]. Guanine and adenine are important bases found both in DNA and RNA, abnormal changes suggesting the deficiency and mutation of the immunity system or the presence of various diseases. Electrochemical detection methods can be employed for all these analytes.

Electrochemical sensors based on polythionine and CNT for nucleic acid bases' determination, are PTH/MWCNT/GCE [79] and PTH/NPAu/MWCNT/GCE [78], both containing poly(thionine).

Uracil has been determined by DPV at PTH/MWCNT/GCE in 0.1 M KCl with a linear response over the concentration range from 10 μM to 550 mM, the detection limit being 0.2 μM and sensitivity 703 $\mu A\,mM^{-1}\,cm^{-2}$ [79].

Good separation of guanine (E_p = 0.62 V) and adenine (E_p = 0.91 V) was obtained by CV at PTH/AuNP/MWCNT/GCE in 0.1 M PBS pH 7.0 [78], both undergoing irreversible oxidation. The peak currents of

guanine and adenine were directly proportional to the scan rate. The pH linear dependence of adenine and guanine oxidation peak potentials had the slopes ~60 mV pH^{-1}, showing that two protons are involved in the mechanism. The oxidation of adenine and guanine at these electrodes follows a two-step mechanism involving a total of $4e^-$ with the first $2e^-$ being lost in the rate-determining step. Guanine and adenine were determined by DPV with a linear response between 0.01–10 μM and 0.05–5.0 μM. The sensitivities were 56.7 and 5.33 μA cm^{-2} μM^{-1} and detection limits 10 and 8.0 nM, respectively.

4.12. Other applications

A PBCB/MWCNT/GCE modified electrode was used as a persulfate sensor, which showed a lower overpotential and higher current response compared with that at bare and PBCB modified electrodes. The amperometric persulfate sensor operated at −0.03 V vs. Ag/AgCl, in PBS pH 7.0, having sensitivities of 124.5 and 21.2 μA mM^{-1} cm^{-2} for the linear concentration range of 10–100 μM and 3.1–1.0 mM, and detection limit of 1 μM [35].

PBCB was also used together with MWCNT for Vitamin B9 (folic acid) detection, the PBCB/MWCNT/GCE exhibiting electrocatalytic activity toward folic acid oxidation. The sensitivity of the PBCB/MWCNT/GCE was 177 μA mM^{-1} cm^{-2}, higher than the values obtained for PBCB/GCE and MWCNT/GCE, of 0.75 and 148 μA mM^{-1} cm^{-2}. The detection limit was 76 μM, lower than that of the other two modified electrodes [36].

Lastly, PBCB was used as a substitute for platinum to construct a low-cost cathode in dye-sensitized solar cells, showing a high electrocatalytic activity for the I_3^-/I^- redox reaction. It was stressed that the overall energy conversion efficiency of the solar cells increases with the amount of polymerized PBCB on MWCNT/GCE [34].

PMalG has been used together with MWCNT for the detection of *p*-nitrophenol, catechol and quinol. The *p*-nitrophenol sensor had a sensitivity of 5 μM, and a linear range up to 1.0 mM [43]. Simultaneous detection of catechol and quinol was done by using DPV in H_2SO_4 aqueous solution pH 1.5, the sensitivities being 0.4 and 3.2 μA cm^{-2} mM^{-1} and detection limits of 5.8 and 1.6 μM, for catechol and quinol, respectively [42].

A sensor for the anticancer drug, irinotecan, was based on PMB/MWCNT/GCE, which had a linear range between 8.0 and 80 μM, with a detection limit of 0.2 μM [47]. PMB was also used for the construction of an aptasensor for thrombin, which was able to detect thrombin in the concentration range 1 nM–1 mM with a limit of detection of 0.7 nM and 0.5 nM by monitoring resistance and capacitance changes, respectively [48].

5. Conclusions

Sensors based on poly(phenazines) or poly(triphenylmethanes) together with CNT constitute a very wide category of analytical tools, being very appropriate for the design of electrochemical (bio) sensors. The high electrocatalytic activity and fast electron transfer rate together with the very good stability of poly(phenazine)/CNT and polytriphenylmethane)/CNT composites indicates their suitability as electrochemical (bio) sensing devices. Current developments are focused on the possibilities of tailoring their individual and combined 3D structure in order to achieve new improved modified electrodes. The present review underlines not only the unique physico-chemical properties of the constituent components, but also possible synergistic effects, which lead to numerous electrochemical (bio) sensors covering a wide variety of applications. Future research may facilitate the development of advanced sensors with applications in the food industry, clinical and point-of-care diagnostics and in the design of biofuel cells.

Acknowledgements

Financial support from Fundação para a Ciência e a Tecnologia (FCT), Portugal PTDC/QUI-QUI/116091/2009, POCH, POFC-QREN (co-financed by FSE and European Community FEDER funds through the program COMPETE and FCT project PEst-C/EME/UI0285/2013) is gratefully acknowledged. M.M.B. and M.E.G. thank FCT for postdoctoral fellowships SFRH/BPD/72656/2010 and SFRH/BPD/36930/2007.

References

[1] C. Li, H. Bai, G.Q. Shi, Conducting polymer nanomaterials, Chem. Soc. Rev. 38 (2009) 2397–2409.
[2] M. Ates, A review study of (bio) sensor systems based on conducting polymers, Mater. Sci. Eng. C 33 (2013) 1853–1859.
[3] G.A. Rivas, M.D. Rubianes, M.C. Rodríguez, N.F. Ferreyra, G.L. Luque, M.L. Pedano, S.A. Miscoria, C. Parrado, Carbon nanotubes for electrochemical biosensing, Talanta 74 (2007) 291–307.
[4] T. Kurkina, A. Vlandas, A. Ahmad, K. Kern, K. Balasubramanian, Label-free detection of few copies of DNA with carbon nanotube impedance biosensors, Angew. Chem. Int. Ed. 50 (2011) 3710–3714.
[5] M.F.L. De Volder, S.H. Tawfick, R.H. Baughman, A.J. Hart, Carbon nanotubes: present and future commercial applications, Science 339 (2013) 535–539.
[6] M.C. Kum, K.A. Joshi, W. Chen, N.V. Myung, A. Mulchandani, Biomolecules-carbon nanotubes doped conducting polymer nanocomposites and their sensor application, Talanta 74 (2007) 370–375.
[7] U. Yogeswaran, S.M. Chen, Separation and concentration effect of f-MWCNTs on electrocatalytic responses of ascorbic acid, dopamine and uric acid at f-MWCNTs incorporated with poly(neutral red) composite films, Electrochim. Acta 52 (2007) 5985–5996.
[8] A. Chen, S. Chatterjee, Nanomaterials based electrochemical sensors for biomedical applications, Chem. Soc. Rev. 42 (2013) 5425–5438.
[9] D. Tasis, N. Tagmatarchis, A. Bianco, M. Prato, Chemistry of carbon nanotubes, Chem. Rev. 106 (2006) 1105–1136.
[10] M. Holzinger, O. Vostrowsky, A. Hirsch, F. Hennrich, M. Kappes, R. Weiss, F. Jellen, Sidewall functionalization of carbon nanotubes, Angew. Chem. Int. Ed. 40 (2001) 4002–4005.
[11] H. Zhang, H. Guo, X. Deng, P. Gu, Z. Chen, Z. Jiao, Functionalization of multi-walled carbon nanotubes via surface unpaired electrons, Nanotechnology 21 (2010) 85706–85707.
[12] K. Mylvaganam, L.C. Zhang, Fabrication and application of polymer composites comprising carbon nanotubes, Recent Pat. Nanotechnol. 1 (2007) 59–65.
[13] A. Le Goff, M. Holzinger, S. Cosnier, Enzymatic biosensors based on SWCNT-conducting polymer electrodes, Analyst 136 (2011) 1279–1287.
[14] H. Dai, Carbon nanotubes: synthesis, integration, and properties, Acc. Chem. Res. 35 (2002) 1035–1044.
[15] A. Star, J.F. Stoddart, D. Steuerman, M. Diehl, A. Boukai, E.W. Wong, X. Yang, S.-W. Chung, H. Choi, J.R. Heath, Preparation and properties of polymer-wrapped single-walled carbon nanotubes, Angew. Chem. Int. Ed. 40 (2001) 1721–1725.
[16] Q. Li, J. Zhang, H. Yan, M. He, Z. Liu, Thionine-mediated chemistry of carbon nanotubes, Carbon 42 (2004) 287–291.
[17] J. Zhang, J.K. Lee, Y. Wu, R.W. Murray, Photoluminescence and electronic interaction of anthracene derivatives adsorbed on sidewalls of single-walled carbon nanotubes, Nano Lett. 3 (2003) 403–407.
[18] J. Liu, A.G. Rinzler, H. Dai, J.H. Hafner, R.K. Bradley, P.J. Boul, A. Lu, T. Iverson, K. Shelimov, C.B. Huffman, F. Rodriguez-Macias, Y.-S. Shon, T.R. Lee, D.T. Colbert, R.E. Smalley, Fullerene pipes, Science 280 (1998) 1253–1255.
[19] T. Ramanathan, F.T. Fisher, R.S. Ruoff, L.C. Brinson, Amino-functionalized carbon nanotubes for binding to polymers and biological systems, Chem. Mater. 17 (2005) 1290–1295.
[20] M. Soleimani, M.G. Afshar, A. Sedghi, Amino-functionalization of multiwall carbon nanotubes and its use for solid phase extraction of mercury ions from fish sample, ISRN Nanotechnol. 2013 (2013) Article ID 674289.
[21] S. Khalili, A.A. Ghoreyshi, M. Jahanshahi, K. Pirzadeh, Enhancement of carbon dioxide capture by amine-functionalized multi-walled carbon nanotube, Clean – Soil Air Water 41 (2013) 939–948.
[22] L. Agüí, P. Yáñez-Sedeño, J.M. Pingarrón, Role of carbon nanotubes in electroanalytical chemistry, a review, Anal. Chim. Acta 622 (2008) 11–47.
[23] S.A. Kumar, S.-M. Chen, Electroanalysis of NADH using conducting and redox active polymer/carbon nanotubes modified electrodes – a review, Sensors 8 (2008) 739–766.
[24] R. Pauliukaite, M.E. Ghica, M.M. Barsan, C.M.A. Brett, Phenazines and polyphenazines in electrochemical sensors and biosensors, Anal. Lett. 43 (2010) 1588–1608.

[25] A.A. Karyakin, E.E. Karyakina, H.-L. Schmidt, Electropolymerized azines: a new group of electroactive polymers, Electroanalysis 11 (1999) 149–155.
[26] A.A. Karyakin, E.E. Karyakina, W. Schuhmann, H.-L. Schmidt, Electropolymerized azines: part II. In a search of the best electrocatalyst of NADH oxidation, Electroanalysis 11 (1999) 553–557.
[27] K. Esumi, M. Ishigami, A. Nakajima, K. Sawada, H. Honda, Chemical treatment of carbon nanotubes, Carbon 34 (1996) 279–281.
[28] C. Ge, F. Lao, W. Li, Y. Li, C. Chen, Y. Qui, X. Mao, B. Li, Z. Chai, Y. Zhao, Quantitative analysis of metal impurities in carbon nanotubes: efficacy of different pretreatment protocols for ICPMS spectroscopy, Anal. Chem. 80 (2008) 9426–9434.
[29] R. Verdejo, S. Lamoriniere, B. Cottam, A. Bismarck, M. Shaffer, Removal of oxidation debris from multi-walled carbon nanotubes, Chem. Comm. 5 (2007) 513–515.
[30] M. Chen, J.-Q. Xu, S.-N. Ding, D. Shan, H.-G. Xue, S. Cosnier, M. Holzinger, Poly (brilliant cresyl blue) electrogenerated on single–walled carbon nanotubes modified electrode and its application in mediated biosensing system, Sens. Actuators B 152 (2011) 14–20.
[31] M.E. Ghica, C.M.A. Brett, The influence of carbon nanotubes and polyazine redox mediators on the performance of amperometric enzyme biosensors, Microchim. Acta 170 (2010) 257–265.
[32] D.-W. Yang, H.-H. Liu, Poly(brilliant cresyl blue)-carbon nanotube modified electrodes for determination of NADH and fabrication of ethanol dehydrogenase-based biosensor, Biosens. Bioelectron. 25 (2009) 733–738.
[33] H.-J. Liu, D.-W. Yang, H.-H. Liu, A hydrogen peroxide sensor based on the nanocomposites of poly(brilliant cresyl blue) and single walled-carbon nanotubes, Anal. Methods 4 (2012) 1421–1426.
[34] K.-C. Lin, J.-Y. Huang, S.-M. Chen, A low cost counter electrode using poly (brilliant cresyl blue) and multi-walled carbon nanotubes for dye-sensitized solar cells, Int. J. Electrochem. Sci. 7 (2012) 12786–12795.
[35] K.-C. Lin, J.-Y. Huang, S.-M. Chen, Poly(brilliant cresyl blue) electrodeposited on multi-walled carbon nanotubes modified electrode and its application for persulfate determination, Int. J. Electrochem. Sci. 7 (2012) 9161–9173.
[36] Y. Umasankar, T.-W. Ting, S.-M. Chen, Characterization of poly(brilliant cresyl blue)-multiwall carbon nanotube composite film and its application in electrocatalysis of vitamin B9 reduction, J. Electrochem. Soc. 158 (2011) K117–K122.
[37] H. Yi, D. Zheng, C. Hu, S. Hu, Functionalized multiwalled carbon nanotubes through in situ electropolymerization of brilliant cresyl blue for determination of epinephrine, Electroanalysis 20 (2008) 1143–1146.
[38] M.E. Ghica, Y. Wintersteller, C.M.A. Brett, Poly(brilliant green)/carbon nanotube-modified carbon film electrodes and application as sensors, J. Solid State Electrochem. 17 (2013) 1571–1580.
[39] V. Pifferi, M.M. Barsan, M.E. Ghica, L. Falciola, C.M.A. Brett, Synthesis characterization and influence of poly(brilliant green) on the performance of different electrode architectures based on carbon nanotubes and poly(3,4-ethylenedioxythiophene), Electrochim. Acta 98 (2013) 199–207.
[40] M.E. Ghica, C.M.A. Brett, Poly(brilliant green) and poly(thionine) modified carbon nanotube coated carbon film electrodes for glucose and uric acid biosensors, Talanta 130 (2014) 198–206.
[41] Y. Umasankar, A.P. Periasamy, S.-M. Chen, Poly(malachite green) at Nafion doped multi-walled carbon nanotube composite film for simple aliphatic alcohols sensor, Talanta 80 (2010) 1094–1101.
[42] Y. Umasankar, A.P. Periasamy, S.-M. Chen, Electrocatalysis and simultaneous determination of catechol and quinol by poly(malachite green) coated multiwalled carbon nanotube film, Anal. Biochem. 411 (2011) 71–79.
[43] Q. Wan, F. Yu, P. Yang, L. Li, The electrochemical behavior and determination of p-nitrophenol based on poly-malachite green/multi-walled carbon nanotube composite film modified electrode, Conf. Environ. Poll. Public Health 1–2 (2010) 900–903.
[44] J.B. Raoof, R. Ojani, M. Baghayeri, Fabrication of layer-by-layer deposited films containing carbon nanotubes and poly(malachite green) as a sensor for simultaneous determination of ascorbic acid epinephrine, and uric acid, Turk. J. Chem. 37 (2013) 36–50.
[45] J.-Y. Wang, P.-C. Nien, C.-H. Chen, L.-C. Chen, K.-C. Ho, A glucose bio-battery prototype based on a GlcDH/(polymethylene blue) bioanode and a graphite cathode with an iodide/tri-iodide redox couple, Bioresour. Technol. 116 (2012) 502–506.
[46] Y. Li, X. Liu, X. Zeng, X. Liu, L. Tao, W. Wei, S. Luo, Construction of poly (methylene blue) on carbon nanotubes ionic liquid paste electrode for sensitive detection of nitrite, Sens. Lett. 8 (2010) 584–590.
[47] N. Karadas, S. Sanli, B. Akmese, B. Dogan-Topal, A. Can, S.A. Ozkan, Analytical application of poly methylene blue-multiwalled carbon nanotubes modified glassy carbon electrode on anticancer drug irinotecan and determination of its ionization constant value, Talanta 115 (2013) 911–919.
[48] A.V. Porfireva, G.A. Evtugyn, A.N. Ivanov, T. Hianik, Impedimetric aptasensors based on carbon nanotubes-poly(methylene blue) composite, Electroanalysis 22 (2010) 2187–2195.
[49] U. Yogeswaran, S.-M. Chen, Multi-walled carbon nanotubes with poly (methylene blue) composite film for the enhancement and separation of electroanalytical responses of catecholamine and ascorbic acid, Sens. Actuators B 130 (2008) 739–749.
[50] R.C. Peña, M. Bertotti, C.M.A. Brett, Methylene blue/multiwall carbon nanotube modified electrode for the amperometric determination of hydrogen peroxide, Electroanalysis 23 (2011) 2290–2296.
[51] D. Wen, L. Deng, M. Zhou, S. Guo, L. Shang, G. Xu, S. Dong, A biofuel cell with a single-walled carbon nanohorn-based bioanode operating at physiological condition, Biosens. Bioelectron. 25 (2010) 1544–1547.
[52] M.M. Barsan, E.M. Pinto, C.M.A. Brett, Electrosynthesis and electrochemical characterisation of phenazine polymers for application in biosensors, Electrochim. Acta 53 (2008) 3973–3982.
[53] H. Li, K.E. Worley, S. Calabrese Barton, Quantitative analysis of bioactive NAD^+ regenerated by NADH electro-oxidation, ACS Catal. 2 (2012) 2572–2576.
[54] J. Yu, M. Rasmussen, S.D. Minteer, Effects of carbon nanotube paper properties on enzymatic bioanodes, Electroanalysis 25 (2013) 1130–1134.
[55] C.W. Narváez-Villarrubia, S.O. Garcia, C. Lau, P. Atanassov, Biofuel cell anodes integrating NAD^+-dependent enzymes and multiwalled carbon nanotube papers, ECS J. Solid State Sci. Technol. 2 (2013) M3156–M3159.
[56] P.G. Fenga, F.P. Cardoso, S. Aquino Neto, A.R. De Andrade, Multiwalled carbon nanotubes to improve ethanol/air biofuel cells, Electrochim. Acta 106 (2013) 109–113.
[57] R.A. Rincón, C. Lau, K.E. Garcia, P. Atanassov, Flow-through 3D biofuel cell anode for NAD^+-dependent enzymes, Electrochim. Acta 56 (2011) 2503–2509.
[58] Z. Wang, M. Etienne, V. Urbanova, G.-W. Kohring, A. Walcarius, Reagentless D-sorbitol biosensor based on D-sorbitol dehydrogenase immobilized in a sol–gel carbon nanotubes-poly(methylene green) composite, Anal. Bioanal. Chem. 405 (2013) 3899–3906.
[59] Z. Wang, M. Etienne, S. Pöller, W. Schuhmann, G.-W. Kohring, V. Mamane, A. Walcarius, Dehydrogenase-based reagentless biosensors: electrochemically assisted deposition of sol–gel thin films on functionalized carbon nanotubes, Electroanalysis 24 (2012) 376–385.
[60] H. Li, H. Wen, S. Calabrese Barton, NADH oxidation catalyzed by electropolymerized azines on carbon nanotube modified electrodes, Electroanalysis 24 (2012) 398–406.
[61] P. Du, P. Wu, C. Cai, A glucose biosensor based on electrocatalytic oxidation of NADPH at single-walled carbon nanotubes functionalized with poly(Nile blue A), J. Electroanal. Chem. 624 (2008) 21–26.
[62] P. Du, S. Liu, P. Wu, C. Cai, Single-walled carbon nanotubes functionalized with poly(Nile blue A) and their application to dehydrogenase-based biosensors, Electrochim. Acta 53 (2007) 1811–1823.
[63] D. Kul, M.E. Ghica, R. Pauliukaite, C.M.A. Brett, A novel amperometric sensor for ascorbic acid based on poly(Nile blue A) and functionalised multi-walled carbon nanotube modified electrodes, Talanta 111 (2013) 76–84.
[64] D. Kul, C.M.A. Brett, Electrochemical investigation and determination of levodopa on poly(Nile blue-A)/multiwalled carbon nanotube modified glassy carbon electrodes, Electroanalysis 26 (2014) 1320–1325.
[65] D. Kul, C.M.A. Brett, Electroanalytical characterisation of dopa decarboxylase inhibitors carbidopa and benserazide on multiwalled carbon nanotube and poly(Nile blue A) modified glassy carbon electrodes, Int. J. Electrochem. 2011 (2011) Article ID 185864, 7 pages.
[66] P. Du, Y.M. Shi, P. Wu, Y.M. Zhou, C.-X. Cai, Rapid functionalization of carbon nanotube and its electrocatalysis, Front. Chem. China 2 (2007) 369–377.
[67] W.-J. Chen, J.-Y. Qu, Glucose oxidase biosensor based on carbon nanotubes and chitosan through electrostatic adsorption, Chin. J. Anal. Chem. 37 (2009) 733–736.
[68] F. Qu, M. Yang, J. Chen, G. Shen, R. Yu, Amperometric biosensors for glucose based on layer-by-layer assembled functionalized carbon nanotube and poly (neutral red) multilayer film, Anal. Lett. 39 (2006) 1785–1799.
[69] U. Yogeswaran, S.-M. Chen, Electrocatalytic properties of electrodes which are functionalized with composite films of f-MWCNT incorporated with poly (neutral red), J. Electrochem. Soc. 154 (2007) E178–E186.
[70] K.C. Lin, J.Y. Huang, S.M. Chen, Enhancing electro-codeposition and electrocatalytic properties of poly(neutral red) and FAD to determine NADH and H_2O_2 using amino-functionalized multi-walled carbon nanotubes, RSC Adv. 3 (2013) 25727–25734.
[71] Y. Zhang, R. Yuan, Y. Chai, Y. Xiang, C. Hong, X. Ran, An amperometric hydrogen peroxide biosensor based on the immobilization of HRP on multi-walled carbon nanotubes/electro-copolymerized nano-Pt-poly(neutral red) composite membrane, Biochem. Eng. J. 51 (2010) 102–109.
[72] R.C. Carvalho, C. Gouveia-Caridade, C.M.A. Brett, Glassy carbon electrodes modified by multiwalled carbon nanotubes and poly(neutral red): a comparative study of different brands and application to electrocatalytic ascorbate determination, Anal. Bioanal. Chem. 398 (2010) 1675–1685.
[73] M.E. Ghica, C.M.A. Brett, Development of novel glucose and pyruvate biosensors at poly(neutral red) modified carbon film electrodes. Applications to natural samples, Electroanalysis 18 (2006) 748–756.
[74] H. Feng, H. Wang, Y. Zhang, B. Yan, G. Shen, R. Yu, A direct electrochemical biosensing platform constructed by incorporating carbon nanotubes and gold nanoparticles onto redox poly(thionine) film, Anal. Sci. 23 (2007) 235–239.
[75] N. Mai, X. Liu, X. Zeng, L. Xing, W. Wei, S. Luo, Electrocatalytic oxidation of the reduced nicotinamide adenine dinucleotide at carbon ionic liquid electrode modified with polythionine/multi-walled carbon nanotubes composite, Microchim. Acta 168 (2010) 215–220.
[76] C. Deng, J. Chen, Z. Nie, M. Yang, S. Si, Electrochemical detection of nitrite based on the polythionine/carbon nanotube modified electrode, Thin Solid Films 520 (2012) 7026–7029.

[77] J.A. Rather, S. Pilehvar, K. De Wael, A biosensor fabricated by incorporation of a redox mediator into a carbon nanotube/Nafion composite for tyrosinase immobilization: detection of matairesinol an endocrine disruptor, Analyst 138 (2013) 204–210.
[78] H. Liu, G. Wang, D. Chen, W. Zhang, C. Li, B. Fang, Fabrication of polythionine/NPAu/MWNTs modified electrode for simultaneous determination of adenine and guanine in DNA, Sens. Actuators B 128 (2008) 414–421.
[79] H. Liu, G. Wang, J. Hu, D. Chen, W. Zhang, B. Fang, Electrocatalysis and determination of uracil on polythionine/multiwall carbon nanotubes modified electrode, J. Appl. Polym. Sci. 107 (2008) 3173–3178.
[80] Q. Mi, Z.W. Wang, C.Y. Chai, J. Zhang, B. Zhao, C.Y. Chen, Multilayer structured immunosensor based on a glassy carbon electrode modified with multi-wall carbon nanotubes polythionine, and gold nanoparticles, Microchim. Acta 173 (2011) 459–467.
[81] Y. Xu, X. Zhang, Y. Wang, P. He, Y. Fang, Enhancement of electrochemical capacitance of carbon nanotubes by polythionine modification, Chin. J. Chem. 28 (2010) 417–421.
[82] R. Yang, C.M. Ruan, W.L. Dai, J.Q. Deng, J.L. Kong, Electropolymerization of thionine in neutral aqueous media and H_2O_2 biosensor based on poly (thionine), Electrochim. Acta 44 (1998) 1585–1596.
[83] Y.-L. Yao, K.-K. Shiu, Low potential detection of glucose at carbon nanotube modified glassy carbon electrode with electropolymerized poly(toluidine blue O) film, Electrochim. Acta 53 (2007) 278–284.
[84] W. Wang, F. Wang, Y. Yao, S. Hu, K.-K. Shiu, Amperometric bienzyme glucose biosensor based on carbon nanotube modified electrode with electropolymerized poly(toluidine blue O) film, Electrochim. Acta 55 (2010) 7055–7060.
[85] H. Li, H. Wen, S. Calabrese Barton, NADH oxidation catalyzed by electropolymerized azines on carbon nanotube modified electrodes, Electroanalysis 24 (2012) 398–406.
[86] J. Zeng, W. Wei, L. Wu, X. Liu, K. Liu, Y. Li, Fabrication of poly(toluidine blue O)/carbon nanotube composite nanowires and its stable low-potential detection of NADH, J. Electroanal. Chem. 595 (2006) 152–160.
[87] Y.-J. Chang, A.P. Periasamy, S.-M. Chen, Poly(toluidine blue) and zirconia nanoparticles electrochemically deposited at gelatin-multiwalled carbon nanotube film for amperometric H_2O_2 sensor, Int. J. Electrochem. Sci. 6 (2011) 4188–4203.
[88] W. Zheng, Y.F. Zheng, Gelatin-functionalized carbon nanotubes for the bioelectrochemistry of hemoglobin, Electrochem. Commun. 9 (2007) 1619–1623.
[89] D. Gligor, A. Walcarius, Glassy carbon electrode modified with a film of poly (toluidine blue O) and carbon nanotubes for nitrite detection, J. Solid State Electrochem. 18 (2014) 1519–1528.
[90] C.-X. Cai, K.-H. Xue, Electrochemical polymerization of toluidine blue O and its electrocatalytic activity toward NADH oxidation, Talanta 147 (1998) 1107–1119.
[91] D.-M. Zhou, J.-J. Sun, H.-Y. Chen, H.-Q. Fang, Electrochemical polymerization of toluidine blue and its application for the amperometric determination of β-D-glucose, Electrochim. Acta 43 (1998) 1803–1809.
[92] J. Zeng, W. Wei, X. Zhai, P. Yang, J. Yin, L. Wu, X. Liu, K. Liu, S. Gong, Assemble-electrodeposited ultrathin conducting poly(azure A) at a carbon nanotube-modified glassy carbon electrode, and its electrocatalytic properties to the reduction of nitrite, Microchim. Acta 155 (2006) 379–386.
[93] Y. Sha, Q. Gao, B. Qi, X. Yang, Electropolymerization of Azure B on a screen-printed carbon electrode and its application to the determination of NADH in a flow injection analysis system, Microchim. Acta 148 (2004) 335–341.
[94] Q. Gao, M. Sun, P. Peng, H. Qi, C. Zhang, Electro-oxidative polymerization of phenothiazine dyes into a multilayer-containing carbon nanotube on a glassy carbon electrode for the sensitive and low-potential detection of NADH, Microchim. Acta 168 (2010) 299–307.
[95] F.S. Saleh, T. Okajima, F. Kitamura, L. Mao, T. Ohsaka, Poly(phenosafranin)-functionalized single-walled carbon nanotube as nanocomposite electrocatalysts: Fabrication and electrocatalysis for NADH oxidation, Electrochim. Acta 56 (2011) 4916–4923.
[96] C.H. Yang, Q. Lu, S.S. Hu, A novel nitrite amperometric sensor and its application in food analysis, Electroanalysis 18 (2006) 2188–2193.
[97] M.M. Barsan, E.M. Pinto, M. Florescu, C.M.A. Brett, Development and characterization of a new conducting carbon composite electrode, Anal. Chim. Acta 635 (2009) 71–78.
[98] C. Yang, J. Yi, X. Tang, G. Zhou, Y. Zeng, Studies on the spectroscopic properties of poly(neutral red) synthesized by electropolymerization, React. Funct. Polym. 66 (2006) 1336–1341.
[99] K. Tanaka, S. Ikeda, N. Oyama, K. Tokuda, T. Ohsaka, Preparation of poly (thionine)-modified electrode and its application to an electrochemical detector for flow-injection analysis of NADH, Anal. Sci. 9 (1993) 783–789.
[100] D.R.S. Jeykumari, S. Ramaprabhu, S.S. Narayanan, A thionine functionalized multiwalled carbon nanotube modified electrode for the determination of hydrogen peroxide, Carbon 45 (2007) 1340–1353.
[101] C.-X. Cai, K.-H. Xue, Chin, Electrocatalytic oxidation of NADH at glassy carbon electrodes modified with an electropolymerized film of Nile blue, Chin. J. Chem. 18 (2000) 182–187.
[102] A.A. Karyakin, E.E. Strakhova, E.E. Karyakina, S.D. Varfolomeyev, A.K. Yatsmirsky, The electrochemical polymerization of methylene blue and bioelectrochemical activity of the resulting film, Bioelectrochem. Bioenerg. 32 (1993) 35–43.
[103] J. Wang, M. Li, Z. Shi, N. Li, Z. Gu, Electrocatalytic oxidation of 3,4-dihydroxyphenylacetic acid at a glassy carbon electrode modified with single-wall carbon, Electrochim. Acta 47 (2001) 651–657.
[104] E. Laviron, General expression of the linear potential sweep voltammogram in the case of diffusionless electrochemical systems, J. Electroanal. Chem. 101 (1979) 19–28.
[105] D. Benito, J.J. Garcı'a-Jareño, J. Navarro-Laboulais, F. Vicente, Electrochemical behaviour of poly(neutral red) on an ITO electrode, J. Electroanal. Chem. 446 (1998) 47–55.
[106] D. Kul, R. Pauliukaite, C.M.A. Brett, Electrosynthesis and characterisation of poly(Nile blue) films, J. Electroanal. Chem. 662 (2011) 328–333.
[107] A. Torstensson, L. Gorton, Catalytic oxidation of NADH by surface-modified graphite electrodes, J. Electroanal. Chem. 130 (1981) 199–207.
[108] Y. Zou, L. Sun, F. Xu, Prussian blue electrodeposited on MWNTs–PANI hybrid composites for H_2O_2 detection, Talanta 72 (2007) 437–442.
[109] C.-M. Chang, Y.-L. Liu, Functionalization of multi-walled carbon nanotubes with non-reactive polymers trough an ozone-mediated process for the preparation of a wide range of high performance/carbon nanotube composites, Carbon 48 (2010) 1289–1297.
[110] J. Wang, J. Dai, T. Yarlagadda, Carbon nanotube–conducting-polymer composite nanowires, Langmuir 21 (2005) 9–12.
[111] C.M.A. Brett, Electrochemical impedance spectroscopy for characterization of electrochemical sensors and biosensors, ECS Trans. 13 (2008) 67–80.
[112] G. Wang, N. Hu, W. Wang, P. Li, H. Gu, B. Fang, Preparation of carbon nanotubes/neutral red composite film modified electrode and its catalysis on rutin, Electroanalysis 22 (2007) 2329–2334.
[113] K.Y. Chun, S.K. Choi, H.J. Kang, C.Y. Park, C.J. Lee, Highly dispersed multi-walled carbon nanotubes in ethanol using potassium doping, Carbon 44 (2006) 1491–1495.
[114] N. Barisci, R. Stella, G.M. Spinks, G.G. Wallace, Characterization of the topography and surface potential of electrodeposited conducting polymer films using atomic force and electric force microscopies, Electrochim. Acta 46 (2000) 519–531.
[115] Y.M. Yan, M.N. Zhang, K.P. Gong, L. Su, Z. Guo, L. Mao, Adsorption of methylene blue dye onto carbon nanotubes: a route to an electrochemically functional nanostructure and its layer-by-layer assembled nanocomposite, Chem. Mater. 17 (2005) 3457–3463.
[116] Y. Zhang, T.H. Pham, M.S. Pena, R.A. Agbaria, I.M. Warner, Spectroscopic studies of brilliant cresyl blue/water-soluble sulfonated calix[4] arene complex, Appl. Spectrosc. 52 (1998) 952–957.
[117] S.A. Kumar, S.F. Wang, Y.T. Chang, Poly(BCB)/Au-nanoparticles hybrid film modified electrode: Preparation, characterization and its application as a non-enzymatic sensor, Thin Solid Films 518 (2010) 5832–5838.
[118] C.J. Collison, M.J. O'Donnell, J.L. Alexander, Complexation between rhodamine 101 and single-walled carbon nanotubes indicative of solvent-nanotube interaction strength, J. Phys. Chem. C 112 (2008) 15144–15150.
[119] J. Wang, Electrochemical glucose biosensors, Chem. Rev. 108 (2008) 814–825.
[120] N.S. Oliver, C. Toumazou, A.E.G. Cass, D.G. Johnston, Glucose sensors: a review of current and emerging technology, Diabet. Med. 26 (2009) 197–210.
[121] S. Kerzenmacher, J. Ducrée, R. Zengerle, F. von Stetten, Energy harvesting by implantable abiotically catalyzed glucose fuel cells, J. Power Sources 182 (2008) 1–17.
[122] Y. Yao, K.K. Shiu, A mediator-free bienzyme amperometric biosensor based on horseradish peroxidase and glucose oxidase immobilized on carbon nanotube modified electrode, Electroanalysis 20 (2008) 2090–2095.
[123] I. Ivanov, T. Vidaković-Koch, K. Sundmacher, Recent advances in enzymatic fuel cells: experiments and modeling, Energies 3 (2010) 803–846.
[124] L. Gorton, P.N. Bartlett, NAD(P)-based biosensors, in: P.N. Bartlett (Ed.), Bioelectrochemistry: Fundamentals, Experimental Techniques and Applications, John Wiley & Sons Ltd., 2008, pp. 157–198.
[125] A. Radoi, D. Compagnone, Recent advances in NADH electrochemical sensing design, Bioelectrochemistry 76 (2009) 126–134.
[126] W. Chen, S. Cai, Q.-Q. Ren, W. Wen, Y.-D. Zhao, Recent advances in electrochemical sensing for hydrogen peroxide: a review, Analyst 137 (2012) 49–58.
[127] M.H. Pournaghi-Azar, R. Ojani, Catalytic oxidation of ascorbic acid by some ferrocene derivative mediators at the glassy carbon electrode. Application to the voltammetric resolution of ascorbic acid and dopamine in the same sample, Talanta 42 (1995) 1839–1848.
[128] J.P. Hart, S.A. Wring, Recent developments in the design and application of screen-printed electrochemical sensors for biomedical environmental and industrial analyses, TrAC Trends Anal. Chem. 16 (1997) 89–103.
[129] C. Pereira, N.R. Ferreira, B.S. Rocha, R.M. Barbosa, J. Laranjinha, The redox interplay between nitrite and nitric oxide: from the gut to the brain, Redox Biol. 1 (2013) 276–284.
[130] P. Capella, B. Ghasemzadech, K. Mitchekk, R.N. Adams, Nafion-coated carbon fiber electrodes for neurochemical studies in brain tissue, Electroanalysis 2 (1990) 175–182.
[131] B.J. Venton, R.M. Wightman, Psychoanalytical electrochemistry: dopamine and behavior, Anal. Chem. 75 (2003) 414A–421A.

[132] M.E. Ghica, C.M.A. Brett, Simple and efficient epinephrine sensor based on carbon nanotube modified carbon film electrodes, Anal. Lett. 46 (2013) 1379–1393.
[133] G. Dryhurst, Electrochemistry of Biological Molecules, Academic Press, New York, 1977.
[134] J.M. Zen, J.J. Jou, G. Ilangovan, Selective voltammetric method for uric acid detection using pre-anodized Nafion-coated glassy carbon electrodes, Analyst 123 (1998) 1345–1350.
[135] J. Chen, C.S. Cha, Detection of dopamine in the presence of a large excess of ascorbic acid by using the powder microelectrode technique, J. Electroanal. Chem. 463 (1999) 93–99.
[136] F.Q. Yang, J. Guan, S.P. Li, Fast simultaneous determination of 14 nucleosides and nucleobases in cultured Cordyceps using ultra-performance liquid chromatography, Talanta 73 (2007) 269–273.